HYDRODYNAMIC ANALYSIS OF OCEAN CURRENT TURBINES USING VORTEX LATTICE METHOD

by

Aneesh Goly

A Thesis Submitted to the Faculty of

The College of Engineering and Computer Science

in Partial Fulfillment of the Requirements for the Degree of

Master of Science

Florida Atlantic University

Boca Raton, Florida

August 2010

HYDRODYNAMIC ANALYSIS OF OCEAN CURRENT TURBINES USING VORTEX LATTICE METHOD

by

Aneesh Goly

This thesis was prepared under the direction of the candidate's thesis advisor, Dr. Palaniswamy Ananthakrishnan, Department of Ocean and Mechanical Engineering, and has been approved by the members of his supervisory committee. It was submitted to the faculty of the College of Engineering and Computer Science and was accepted in partial fulfillment of the requirements for the degree of Master of Science.

SUPERVISORY COMMITTEE:

Palaniswamy Ananthakrishnan, Ph.D.
Thesis Advisor

Manhar R. Dhanak, Ph.D.

Howard Hanson, Ph.D.

Nikolaos I. Xiros, Ph.D.

Mohammad Ilyas, Ph.D.
Chair, Department of Ocean and Mechanical Engineering

Karl K. Stevens, Ph.D., P.E.
Dean, College of Engineering and Computer Science

Barry T. Rosson, Ph.D.
Dean, Graduate College

July 8, 2010
Date

ACKNOWLEDGEMENTS

I would like to express my gratitude to my advisor, Palaniswamy Ananthakrishnan, for his support, patience, and encouragement throughout my graduate studies. It is not often that one finds an advisor who always finds the time for listening to the little problems that unavoidably crop up in the course of performing research. His technical and editorial advice was essential to the completion of this master's thesis and has taught me innumerable lessons and insights.

I would like to sincerely thank my committee members Dr. Dhanak, Dr. Hanson and Dr. Xiros for their valuable comments, suggestions and input to the thesis.

My special thanks go to Ranjith for his encouragement and numerous fruitful discussions related to the research. I feel privileged to have been able to work with Zaqie, Waazim, Lakitosh and Baishali who were encouraging me all through my thesis.

My deepest gratitude goes to my family for their unflagging love and support throughout my life. In the first place to my parents, Srinivas and Rajani for giving me everything in my life. Second, to my grandparents and aunt, Jaishanker, Pushpavathy and Rekha for their unparalleled love and care. Next, to uncle Ravi for his motivation throughout my thesis. Last but not the least, to my uncle Kumar Allady, who directed me in choosing this field and together with aunt, Vishala, has given me unparalleled love, affection and guidance. Finally, I express my gratitude to each and every member in my family, who finds joy in my every success as much. I am proud to have such a family.

The financial support provided by the Center for Ocean Energy Technology of Florida Atlantic University to the author in the form of graduate student research assistantship and tuition waiver for the past two year is gratefully acknowledged.

ABSTRACT

Author: Aneesh Goly

Title: Hydrodynamic Analysis of Ocean Current Turbines using Vortex Lattice Method

Institution: Florida Atlantic University

Thesis Advisor: Dr. Palaniswamy Ananthakrishnan

Degree: Master of Science

Year: 2010

The main objective of the thesis is to carry out a rigorous hydrodynamic analysis of ocean current turbines and determine power for a range of flow and geometric parameters. For the purpose, a computational tool based on the vortex lattice method (VLM) is developed. Velocity of the flow on the turbine blades, in relation to the free-stream velocity, is determined through induction factors. The geometry of trailing vortices is taken to be helicoidal. The VLM code is validated by comparing its results with other theoretical and experimental data corresponding to flows about finite - aspect ratio foils, swept wings and a marine current turbine. The validated code is then used to study the performance of the prototype gulfstream turbine for a range of parameters. Power and thrust coefficients are calculated for a range of tip speed ratios and pitch angles. Of all the cases studied, the one corresponding to tip speed ratio of 8 and uniform pitch angle 2^0 produced the maximum power of 41.3 [kW] in a current of 1.73 [m/s]. The

corresponding power coefficient is 0.45 which is slightly less than the Betz limit power coefficient of 0.5926. The VLM computational tool developed for the research is found to be quite efficient in that it takes only a fraction of a minute on a regular laptop PC to complete a run. The tool can therefore be efficiently used or integrated into software for design optimization.

DEDICATION

This thesis is dedicated to my wonderful family.

"*You have been with me every step of my way, through good and bad times. Thank you for all the unconditional love, guidance, and support that you have always given me, helping me to succeed and instilling in me the confidence that I am capable of doing anything I put my mind to. Thank you for everything. I love you all!*"

HYDRODYNAMIC ANALYSIS OF OCEAN CURRENT TURBINES USING VORTEX LATTICE METHOD

LIST OF FIGURES

CHAPTER 1

INTRODUCTION

The Gulf Stream is a fast, warm and intense ocean current of the northern Atlantic Ocean off eastern North America. It originates in the Gulf of Mexico and passes through the Straits of Florida as Florida current and then flows northward along the southeast coast of the United States. North of Cape Hatteras the Gulf Stream veers northeastward into the Atlantic Ocean, where it splits to form the North Atlantic Drift and the Canary Current (Stommel [1]).

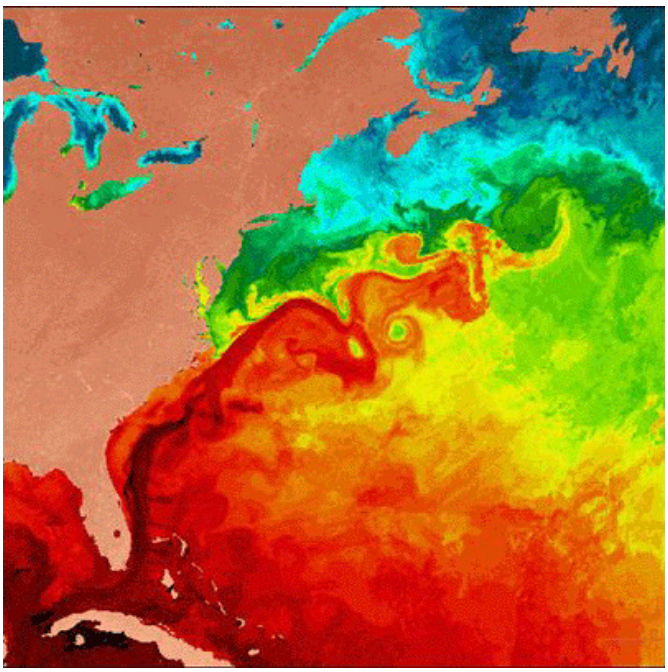

Figure 1.1 The intensification of the gulf stream current

(**Source:** Satellite image from the SeaWifs Imaging Project NASA SeaWiFS [2])

The Gulf Stream is approximately 100 kilometers (62 mi) wide and 800 meters (2,600 ft) to 1,200 meters (3,900 ft) deep. The current velocity is fastest near the surface, with the maximum speeds up to 2.5 meters per second (5.6 mph) (Philips [3]).

Recent study suggests us that the Gulf Stream transports water at a rate of 30 million cubic meters per second (equal to 30 Sverdrup's) through the Florida Straits, the Gulf Stream is one of the most energy dense ocean currents in the world. This, combined with the fact that it passes very close to land along South East Florida, has made the Gulf Stream a highly-potential and economically-feasible source of renewable energy.

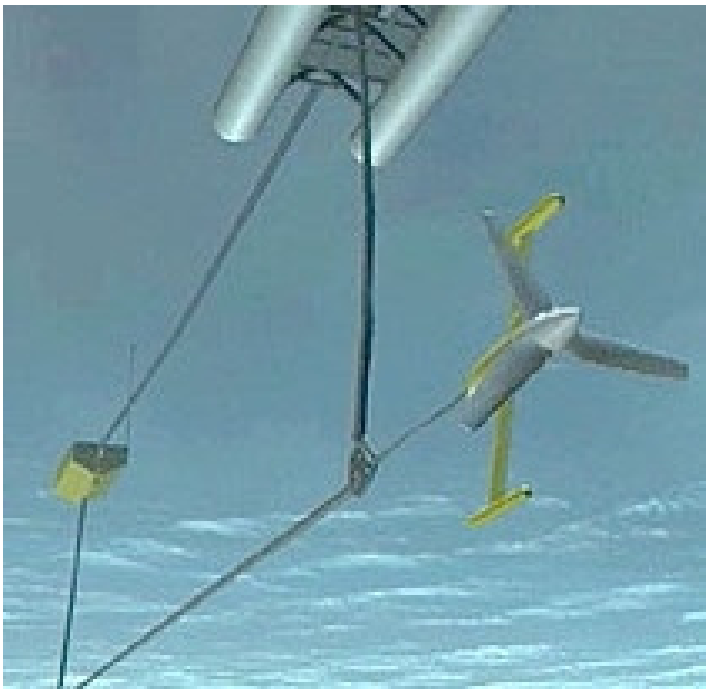

Figure 1.2 Proposed Gulf Stream turbine of Florida Atlantic University

(**Source:** Center for Ocean Energy Technology, FAU COET [6])

1.1 Motivation

At present, the design of wind or current turbines is largely based on formulas such as

$$P = \frac{1}{2}\rho A U^3 4a(1-a)^2 \qquad (1.1)$$

which is obtained using the actuator-disk model (Manwell, et al., [7]). In the above formula,

P is the power generated by the turbine,

ρ is the air density,

A is the cross sectional area of the actuator disk,

U is the air velocity and

a is the axial induction factor

In obtaining the above formula, the turbine is modeled as an "actuator disk" (Figure 1.3) across which velocity is continuous but not the pressure.

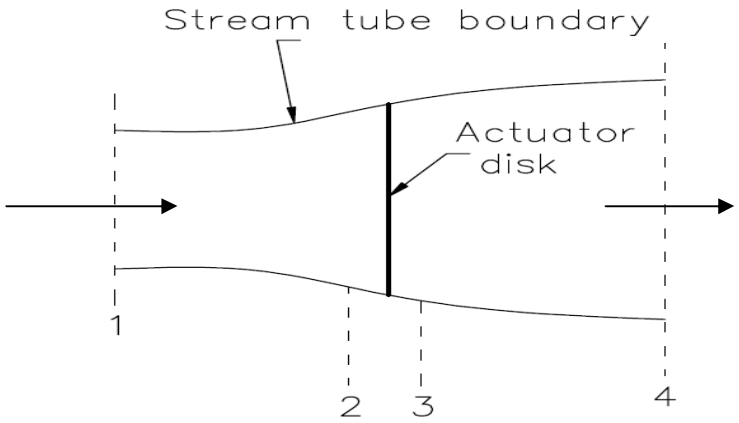

Figure 1.3 Actuator disk model of a wind turbine

In the Figure 1.3, 1, 2, 3 and 4 indicate locations corresponding to upstream, face of the turbine, back of the turbine and downstream, respectively. Using the principles of balance of momentum and energy applied to the flow about the actuator disk, one can derive the turbine power Equation 1.1 as follows (Manwell, et al., [7]).

Let U_t be the velocity across the actuator disk. And from the equation of continuity:

$$U_t A_t = U_1 A_1 = U_4 A_4 \tag{1.2}$$

Where U is the air velocity and A is the area of the respective stations.

Applying the Bernoulli's principle upstream and downstream of the actuator disk we get:

$$Pr_1 + \frac{1}{2}\rho {U_1}^2 = Pr_2 + \frac{1}{2}\rho {U_2}^2 \tag{1.3}$$

$$Pr_3 + \frac{1}{2}\rho {U_3}^2 = Pr_4 + \frac{1}{2}\rho {U_4}^2 \tag{1.4}$$

Where Pr is the pressure and ρ is the density of the fluid.

Assuming $Pr_1 = Pr_4$ and $U_2 = U_3$, from the above two equations we get

$$Pr_2 - Pr_3 = \frac{1}{2}\rho\left({U_1}^2 - {U_4}^2\right) \tag{1.5}$$

Thus,

$$T = (Pr_2 - Pr_3)A_t = \frac{1}{2}\rho A_t\left({U_1}^2 - {U_4}^2\right) = \rho U_t A_t (U_1 - U_4) \tag{1.6}$$

where, $U_t = \frac{U_1 + U_4}{2}$

the power across the disk is given by

$$\begin{aligned} P_t = P_{in} - P_{out} = P_1 - P_4 = \frac{1}{2}\rho {U_1}^2 . A_1 U_1 - \frac{1}{2}\rho {U_4}^2 . A_4 U_4 \\ = \frac{1}{2}\rho U_t A_t \left({U_1}^2 - {U_4}^2\right) \end{aligned} \tag{1.7}$$

Or,

$$P_t = T.U_t = \frac{1}{2}\rho U_t A_t\left({U_1}^2 - {U_4}^2\right) \tag{1.8}$$

The maximum power coefficient is determined by taking derivative of the above equation with respect to the downstream velocity and equating it to zero,

$$\frac{dP_t}{dU_4} = 0$$

$$\frac{d}{dU_4}\left[\frac{1}{2}\rho U_t A_t\left({U_1}^2 - {U_4}^2\right)\right] \tag{1.9}$$

$$= \frac{1}{2}\rho A_t \frac{d}{dU_4}\left[\frac{U_1 + U_4}{2}\left({U_1}^2 - {U_4}^2\right)\right] = 0$$

After doing some algebra we get $U_4/U_1 = -1$ and $1/3$. As we know it cannot be -1, $U_4/U_1 = 1/3$.

i.e. $U_4 = \frac{1}{3}U_1$

Substituting U_4 in the above equation, we get maximum power

$$P_t = \frac{1}{2}\rho.\frac{1}{2}\left(U_1 + \frac{1}{3}U_4\right).A_t.\left({U_1}^2 - \frac{1}{9}{U_1}^2\right)$$

$$= \frac{1}{2}\rho A_t {U_1}^3\left(\frac{1}{2}.\frac{4}{3}.\frac{8}{9}\right) \tag{1.10}$$

The wind turbine performance is usually characterized by its power coefficient, C_P defined as

$$C_P = \frac{P_t}{\frac{1}{2}\rho U^3 A} = \frac{Rotor\ Power}{Power\ in\ the\ wind} \tag{1.11}$$

Finally,

$$C_P = \frac{P_t}{\frac{1}{2}\rho A_t {U_1}^3} = \frac{\frac{1}{2}\rho A_t {U_1}^3 . (\frac{16}{27})}{\frac{1}{2}\rho A_t {U_1}^3} \tag{1.12}$$

where $U = U_1$ and $A = A_t$, and thus the maximum ideal power coefficient turns out to be

$$C_{P,max} = \frac{16}{27} = 0.5926 \tag{1.13}$$

The above formulas are ideal in the sense that they are based on one-dimensional, steady, inviscid flow and that turbine is modeled as disk. Nevertheless, the formula is quite useful for, estimating the upper limit of turbine performance. In the case of ocean turbines, the flow field is highly complex because of possible variability in the current, surface wave effects and ambient turbulence. The applicability of the above formulas for ocean current turbines is therefore doubtful. Also, the applicability has thus far not been validated. Development of a rigorous, and yet computationally efficient, hydrodynamic model for the design and performance-prediction of ocean turbines, as pursued in this thesis, is thus motivated. In particular, the development focuses on determining the following:

- Turbine drag, lift, thrust, torque,
- Turbine power,
- Flow about turbine blades, and
- Principal factors affecting design

1.2 Vortex Lattice Method

In the present thesis, the hydrodynamic model is developed using the vortex lattice method. The vortex lattice method is chosen because of its widely demonstrated accuracy in aerodynamic and hydro/aero foil applications (Katz, et al., [8], Bertin [9], Houghton, et al., [10], Melin [16], Masquelier [17] and Chung [18]). In the VLM, which is an extension of the Prandtl's lifting line theory, the lifting surface is modeled using a lattice of horseshoe vortices, strengths of which are determined based on the no-flux (tangency) flow condition on the surface (Anderson [11]).

The vortex lattice method developed here allows one to determine both the span wise and the chord wise distributions of lift over the blade surfaces. Some of the modifications to be made to the traditional vortex lattice method for modeling the turbine flow include that related to resultant flow due to the current and blade rotation. The wind velocity encountered by an airplane wing is mainly due to upstream flow, whereas the flow velocity encountered by a turbine is resultant of both the ambient current and the rotation of the blade.

Vortex lattice methods have been extensively applied to thin lifting surfaces, typically wings. In the turbine application, the vortex lattice methods have several major advantages over blade element theory (Anderson [11]) which require certain a priori knowledge of lift and drag coefficients and negligible span-wise flow. Vortex lattice methods account for both interference effects due to other blades and three dimensional effects due to a finite aspect ratio without requiring any empirical correction or tuning factors.

The hydrodynamic analysis using vortex lattice method is potentially more useful for studying the ocean current turbine and is also less expensive and time consuming compared to experimental water tunnel tests. The VLM method, of course, cannot predict the flow to a fine detail, as for example pressure fluctuations within turbulent boundary layer, but that is not the purpose of the present thesis. A detailed flow analysis using computationally intensive CFD codes such as FLUENT are also being undertaken in accompanying projects (such as Reza [12]) at Florida Atlantic University. The primary objective of this thesis is to develop a rigorous and yet computationally-efficient algorithms for determining global hydrodynamic characteristics of a turbine such as its torque and power.

1.3 Scope of the Thesis

The tasks and scope of the thesis are as follows:

- Development of algorithm based on VLM for steady flow about turbine blade,
- Determination of lift, drag, thrust, power and respective coefficients of the turbine for a range of current speeds,
- Comparison with empirical turbine equations based on ideal momentum theory and Betz limit,
- Determination of pressure variation over of the turbine blades, and
- Determination of principal parameters affecting performance

The thesis will result in a computational tool that can be used for design improvement and performance assessment of ocean current turbines.

CHAPTER 2

FORMULATION OF THE PROBLEM

In this Chapter, we present the equations governing the flow about an ocean turbine and also hydrodynamic modeling of lifting surfaces using the vortex lattice method. In the formulation, the fluid is assumed to be inviscid and incompressible with vortices (in reality generated by viscosity) treated using potential flow theory.

2.1 Potential Flow

In fluid dynamics, an irrotational flow velocity can be described in terms of velocity potential ϕ, as follows Newman [13]) :

$$V = \nabla\phi \tag{2.1}$$

By the principle of conservation of mass, one obtains the following equation of continuity for an incompressible fluid:

$$\nabla.\bar{V} = 0 \tag{2.2}$$

with

$$\bar{V} = \nabla\phi \tag{2.3}$$

the equation of continuity becomes

$$\nabla^2\phi = 0 \tag{2.4}$$

Upon of solving the above Laplace equation for the velocity potential, subject to appropriate boundary conditions, one can determine the velocity from its gradient and the pressure using the Euler's integral (Bernoulli's equation) which is obtained by spatially integrating the Euler's momentum equation:

$$\int_{\Omega} \left(\frac{\partial\rho\vec{V}}{\partial t} + \nabla.\left(\rho\vec{V}\right)\vec{V}\right) d\Omega = -\int_{S} p\hat{n}\, dS - \int_{\Omega} \rho g\hat{k}\, d\Omega \tag{2.5}$$

which, with $\bar{V} = \nabla\phi$, becomes

$$p = -\rho\left(gz + \frac{\partial\phi}{\partial t} + \frac{1}{2}|\nabla\phi|^2\right) \tag{2.6}$$

2.2 Biot - Savart Law

There are several techniques for solving the Laplace equation and the one considered in the present thesis is based on the distribution of vortices (in particular line vortices). One can determine the velocity field induced by potential line vortex using the Biot-Savart Law. Per Biot-Savart Law, the differential velocity induced at a point due to a vortex filament segment dl of strength Γ is given by,

$$d\vec{V} = \frac{\Gamma \left(\overrightarrow{d\vec{l}} X \bar{r}\right)}{4\pi|\bar{r}|^3} \tag{2.7}$$

For a vortex segment of finite length, integration of the above gives (Houghton, et al., [10])

$$V = \frac{\Gamma}{4\pi r}[\cos\theta_1 - \cos\theta_2] \tag{2.8}$$

where,

Γ is the strength of the vortex,

r is the perpendicular distance between the point and the vortex line,

V is the induced velocity

θ_1 and θ_2 represents the angles between the line and the two ends of the vortex segment (refer to Figure 2.2). In the case of a vortex segment of infinite length, $\theta_1 = \theta_2 = 0$ and therefore

$$V = \frac{\Gamma}{2\pi.r} \tag{2.9}$$

2.3 Horseshoe Vortex

The horseshoe vortex represents a vortex system containing one finite bound vortex and two semi infinite trailing vortices (Figure 2.1). The finite vortex has the two end points in the field, where as the semi infinite vortex has one point in the field and the other extends to infinity. As the name says the shape of the vortex is vaguely reminiscent to a horseshoe.

The finite vortex is called the bound vortex which produces the lift as stated by the Kutta-Joukowski theorem. The semi infinite vortices are called as trailing vortices and responsible for the downwash velocity which induces a drag on the wing. The drag force acting on the wing is lift induced drag and is normal to the lift force. According to Prandtl, the vortex strength (circulation Γ) reducing along the span of the wing is shed in the vortex sheet leaving the trailing edge.

2.4 Velocity Induced by a Horseshoe Vortex

As indicated above the horseshoe vortex consists of three line vortices one corresponding to the bound vortex and the other two to the two trailing vortices. The Biot-Savart law is used to calculate the induced velocity by the three parts of horseshoe vortex. The velocity induced by horseshoe vortex at a point is the sum effect of the three parts. In the vortex lattice method, the mean camber surface of a wing is divided up into several panels and a horseshoe vortex is placed on each of the panels so that the each horseshoe vortex is associated with one lifting panel (Mason [14]). Thus, in the method the wing surface is modeled as a lattice of horseshoe vortices, and hence the name for the method.

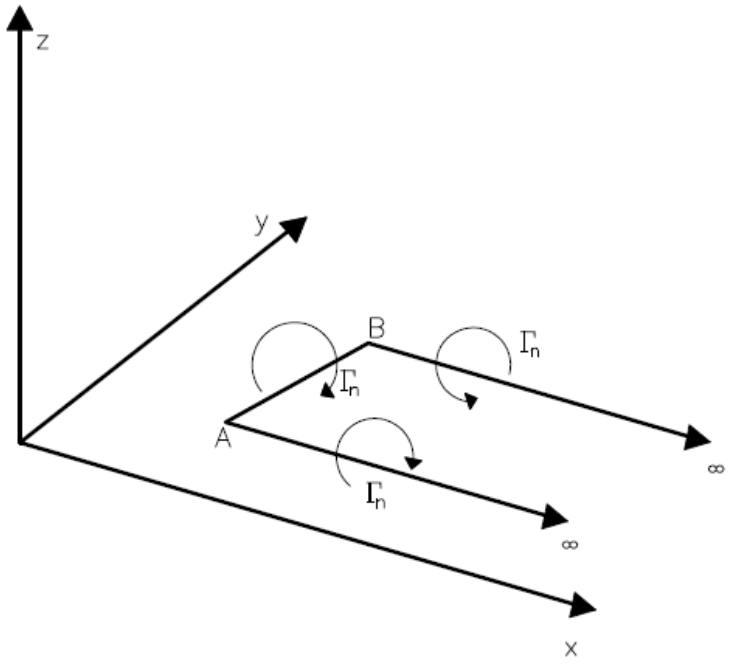

Figure 2.1 The horseshoe vortex with bound vortex AB and the trailing vortices A∞ and B∞.

The Figure 2.1 best describes the geometry of the horse shoe vortex. The bound vortex and the trailing vortices are taken to be straight filaments. For calculating the total induced velocity by the horseshoe vortex it is best if we calculate them separately and then sum it up together. As shown in Figure 2.1, we denote the bound vortex as AB with the vorticity directed from A to B and the induced velocity is denoted by V_{AB}.

Let us consider Figure 2.2 for calculating the induced velocities of the horseshoe. C is an arbitrary point in the space whose coordinates are (x, y, z). The distance of point C from A and B is respectively r_1 and r_2. The normal distance from AB to point C is given as r_n.

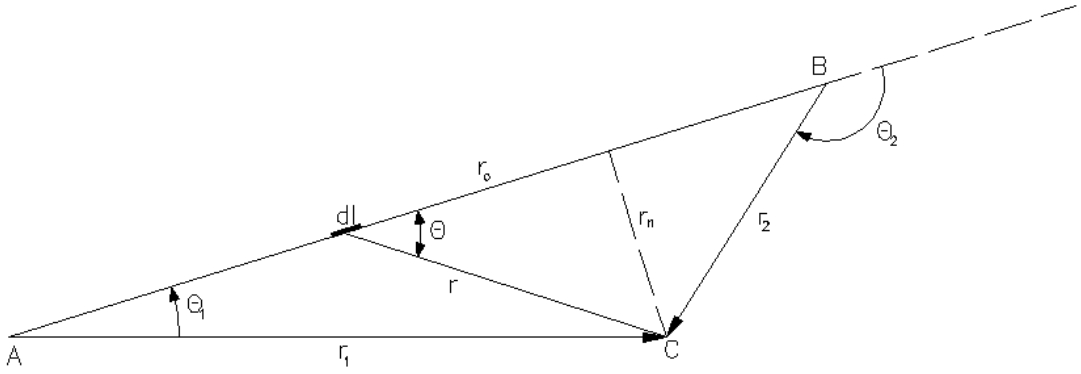

Figure 2.2 The angles and magnitude distribution of the horseshoe vortex

Let dl be the infinitesimal length on AB at a distance r from point C. From geometry,

$$r = \frac{r_n}{\sin\theta}\ , \tag{2.10}$$

$$dl = \frac{r}{\sin\theta}d\theta = \frac{r_n}{\sin\theta^2}d\theta \tag{2.11}$$

The increment in velocity dV at a point C due to the vortex filament dl (Karamcheti [19], Mason [14]) is:

$$dV = \frac{\Gamma}{4\pi}.\frac{dl\ X\ r}{|r|^3} = \frac{\Gamma}{4\pi}.\frac{|dl||r|\sin\theta}{|r|^3}\ \frac{V}{|V|} \tag{2.12}$$

Substituting Equations 2.10 and 2.11 in 2.12, we get

$$dV = \frac{\Gamma}{4\pi}\ \frac{\sin\theta}{r_n}d\theta \tag{2.13}$$

Integrating the above equation, one gets

$$V = \frac{\Gamma}{4\pi r_n}\int_{\theta 1}^{\theta 2}\sin\theta\, d\theta = \frac{\Gamma}{4\pi r_n}(\cos\theta_1 - \cos\theta_2) \tag{2.14}$$

In the vector form, above can be written as

$$\bar{V} = \frac{\Gamma}{4\pi r_n}(\cos\theta_1 - \cos\theta_2)e \tag{2.15}$$

where e is the unit vector along AB.

Note that for an semi infinite vortex filament, θ_1 goes to 0, and $\theta_2$goes to π -θ, and so

$$\bar{V} = \frac{\Gamma}{4\pi r_n}(1 + \cos\theta)e \tag{2.16}$$

This is the two-dimensional solution for induced velocity. Alternately, one can obtain expressions in vector form that is more general in the sense that filament orientations may be arbitrary in the three-dimensional space. Using the vector designations of AB, AC, and BC as shown in Figure 2.2, we can express the following:

$$r_n = \frac{|\bar{r}_1 X \bar{r}_2|}{r_0} \tag{2.17}$$

$$\cos\theta_1 = \frac{\bar{r}_0 . \bar{r}_1}{r_0 r_1} \tag{2.18}$$

$$\cos\theta_2 = \frac{\bar{r}_0 . \bar{r}_2}{r_0 r_2} \tag{2.19}$$

The direction of the induced velocity is described by the unit vector

$$e = \frac{\bar{r}_1 \mathrm{X} \bar{r}_2}{|\bar{r}_1 \mathrm{X} \bar{r}_2|} \tag{2.20}$$

Thus, substituting the above equations in the Equation 2.14

$$\bar{V} = \frac{\Gamma_n}{4\pi} \frac{\bar{r}_1 \mathrm{X} \bar{r}_2}{|\bar{r}_1 \mathrm{X} \bar{r}_2|^2} \left[\bar{r}_0 \left(\frac{\bar{r}_1}{r_1} - \frac{\bar{r}_2}{r_2}\right)\right] \tag{2.21}$$

This is the general form of the equation for the induced velocity due to a line vortex in the vortex lattice method. In the vortex lattice method, the bound filament AB is placed at quarter panel chord (Mason [14]), reason for which is given in Appendix A. For

convenience, in the present work the trailing vortices, if taken to be straight lines, are taken to be parallel to the x-axis.

With the coordinates of points A, B denoted as (x_{1n},y_{1n},z_{1n}) and (x_{2n},y_{2n},z_{2n}) and that of C as (x,y,z), the vector relations for AB, AC and BC becomes

$$\bar{r}_0 = \overline{AB} = (x_{2n} - x_{1n})\bar{\imath} + (y_{2n} - y_{1n})\bar{\jmath} + (z_{2n} - z_{1n})\bar{k}$$

$$\bar{r}_1 = \overline{AC} = (x - x_{1n})\bar{\imath} + (y - y_{1n})\bar{\jmath} + (z - z_{1n})\bar{k} \qquad (2.22)$$

$$\bar{r}_2 = \overline{BC} = (x - x_{2n})\bar{\imath} + (y - y_{2n})\bar{\jmath} + (z - z_{2n})\bar{k}$$

Thus the expression for the velocity at C given in Equation (2.21) becomes, for bound vortex, the following

$$\bar{V}_{AB} = \frac{\Gamma_n}{4\pi}\{\chi\}\{\xi\} \qquad (2.23)$$

where,

$$\chi = \frac{\bar{r}_1 X \bar{r}_2}{|\bar{r}_1 X \bar{r}_2|^2} =$$

$$\frac{\{[(y-y_{1n})(z-z_{2n})-(y-y_{2n})(z-z_{3n})]\hat{\imath}-[(x-x_{1n})(z-z_{2n})-(x-x_{2n})(z-z_{3n})]\hat{\jmath}+[(x-x_{1n})(y-y_{2n})-(x-x_{2n})(y-y_{1n})]\hat{k}\}}{\{[(y-y_{1n})(z-z_{2n})-(y-y_{2n})(z-z_{1n})]^2+[(x-x_{1n})(z-z_{2n})-(x-x_{2n})(z-z_{3n})]^2+[(x-x_{1n})(y-y_{2n})-(x-x_{2n})(y-y_{3n})]^2\}}$$

(2.24)

$$\{\xi\} = \left(\bar{r}_0 . \frac{\bar{r}_1}{r_1} - \bar{r}_0 . \frac{\bar{r}_2}{r_2}\right)$$

$$= \left\{ \frac{[(x_{2n} - x_{1n})(x - x_{1n}) + (y_{2n} - y_{1n})(y - y_{3n}) + (z_{2n} - z_{3n})(z - z_{1n})]}{[(x - x_{1n})^2 + (y - y_{1n})^2 + (z - z_{1n})^2]^{\frac{1}{2}}} \right.$$

$$\left. - \frac{[(x_{2n} - x_{1n})(x - x_{2n}) + (y_{2n} - y_{1n})(y - y_{2n}) + (z_{2n} - z_{1n})(z - z_{2n})]}{[(x - x_{2n})^2 + (y - y_{2n})^2 + (z - z_{2n})^2]^{\frac{1}{2}}} \right\}$$

(2.25)

Next, let us consider the velocity induced by the trailing vortices. To begin, let us consider contribution from the segment AD where the point D is at a distance (x_{1n}- x_{3n}) downstream of A. The velocity induced by the collinear finite length filament AD is given as

$$\bar{r}_0 = \overline{DA} = (x_{1n} - x_{3n})\bar{\imath}$$

$$\bar{r}_1 = (x - x_{3n})\bar{\imath} + (y - y_{1n})\bar{\jmath} + (z - z_{1n})\bar{k} \tag{2.26}$$

$$\bar{r}_2 = (x - x_{1n})\bar{\imath} + (y - y_{1n})\bar{\jmath} + (z - z_{1n})\bar{k}$$

Thus the induced velocity by AD is

$$\bar{V}_{AD} = \frac{\Gamma_n}{4\pi}\{\chi\}\{\xi\} \tag{2.27}$$

where

$$\{\chi\} = \frac{(z - z_{1n})\bar{\jmath} + (y_{1n} - y)\bar{k}}{[(z - z_{1n})^2 + (y_{1n} - y)^2](x_{3n} - x_{1n})} \tag{2.28}$$

and

$$\begin{aligned}&\{\xi\}\\&= (x_{3n}\\&- x_{1n})\left\{\frac{x_{3n} - x}{[(x - x_{3n})^2 + (y - y_{1n})^2 + (z - z_{1n})^2]^{1/2}}\right.\\&\left.+ \frac{x - x_{1n}}{[(x - x_{1n})^2 + (y - y_{1n})^2 + (z - z_{1n})^2]^{1/2}}\right\}\end{aligned} \tag{2.29}$$

In the case of semi-infinite trailing vortices, x_{3n} goes to infinity, thus the first term in the above equation goes to 1(one) and the velocity induced by the trailing vortex filament extending from A to infinity parallel to the x-axis becomes

$$\bar{V}_{A\infty}$$

$$= \frac{\Gamma_n}{4}\left[\frac{(z+z_{1n})\hat{j}+(y_{1n}-y)\hat{k}}{(z+z_{1n})^2+(y_{1n}-y)^2}\right]\left[1 + \frac{x-x_{1n}}{\{(x-x_{1n})^2+(y-y_{1n})^2+(z-z_{1n})^2\}^{1/2}}\right] \tag{2.30}$$

Similarly, the velocity induced by the trailing vortex filament that extends from B to infinity parallel to the x axis is given by

$$\bar{V}_{B\infty}$$

$$= -\frac{\Gamma_n}{4}\left[\frac{(z-z_{2n})\hat{j}+(y_{2n}-y)\hat{k}}{(z-z_{2n})^2+(y_{2n}-y)^2}\right]\left[1 + \frac{x-x_{2n}}{\{(x-x_{2n})^2+(y-y_{2n})^2+(z-z_{2n})^2\}^{1/2}}\right] \tag{2.31}$$

To apply the above expressions for velocity induced by a horseshoe vortex to vortex lattice method, we designate the field point C (x, y, z) to be that of the m^{th} control point with coordinates (x_m, y_m, z_m) and the induced velocity at the m^{th} control point due to the horseshoe vortex representing the n^{th} panel as $V_{m,n}$. Thus,

$$\bar{V}_{m,n} = \overline{V_{AB}} + \overline{V_{A\infty}} + \overline{V_{B\infty}} \tag{2.32}$$

Since induced velocity is a linear function of circulation, the above can be written as

$$\bar{V}_{m,n} = \bar{C}_{m,n}\Gamma_n \tag{2.33}$$

where $\bar{C}_{m,n}$ is the influence coefficient matrix of size m x n. The coefficient matrix depends on the relative geometries of the m^{th} control point and n^{th} horseshoe vortex.

2.5 Boundary Conditions

To find a distribution of circulation on a wing, C_{mn} must be calculated at points where the flow conditions are known. These are control points, located at the mid-panel span-wise and at the three-quarter panel chord length of the panel. If N horseshoe vortices are used to model the flow field, N control points are required to enable the solution of the N simultaneous equations.

The velocity induced at any point in the space is calculated using the Equation 2.33, given the circulation strengths and the geometry of the blade are known. These circulation strengths are not known initially, and a boundary condition is to be established to find these strengths. The boundary condition is based on the no-flux condition on the body surface. In other words, the flow is parallel to the surface at every control point thereby making it a stream surface.

By the no-flux condition of stationary wing gives

$$V.n = 0 \tag{2.34}$$

on the surface. The above equation is satisfied at the control point of each panel. Interpreted differently, the above equation states that the free stream velocity component normal to the lifting surface at the control point must be cancelled by the normal component of the velocity induced by the horseshoe vortices making up the lattice. In case of a cambered wing, referring to Figure 2.3, the tangency condition becomes

$$-U_m \sin\delta + V_m \cos\delta + V_\infty \sin(\alpha - \delta) = 0 \tag{2.35}$$

where, δ is the slope of the mean camber line at control point given by

$$\delta = \tan^{-1}\frac{dZ}{dX} \tag{2.36}$$

U_m and V_m are x and z component of the induced velocity vector $\bar{V}_{m,n}$, V_∞ is the free stream velocity and α is the known angle of attack of the panel.

In the case of small angle of attack and when the slope of the mean camber line is also small, Equation 2.35 further reduces to

$$-U_m\delta + V_m\delta + V_\infty(\alpha - \delta) = 0 \tag{2.37}$$

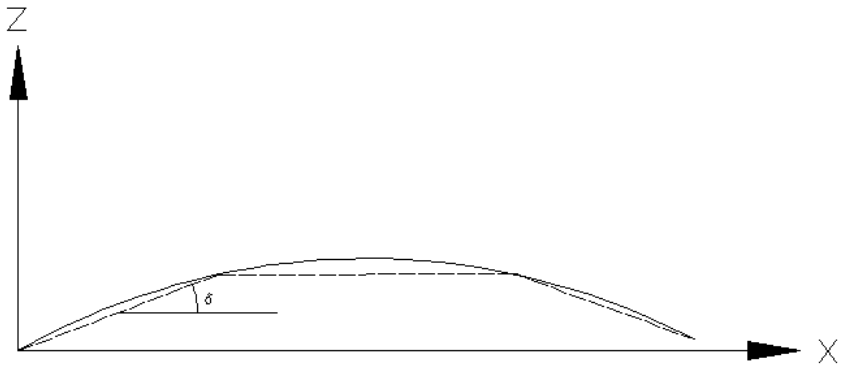

Figure 2.3 Representation of the panel distribution on the cambered wing

In this chapter, we presented formulation of inviscid flow and the possibility of analyzing flow about lifting surfaces using horseshoe vortices. In the next chapter, we will review the vortex lattice method and the algorithms developed in the present thesis for turbine flow analysis.

CHAPTER 3

VORTEX LATTICE METHOD

In this chapter, we present the essentials of the vortex lattice method, in particular the discretization of the lifting surface, solution of the matrix equation for the circulation strengths and the determination of the lift force.

3.1 Generation of Lattice

In vortex lattice method, a lifting surface is divided into a grid in such a way that span wise divisions are made parallel, at least approximately, to free stream streamlines and chord wise divisions are made long constant percent chord lines. In the case of a wing, both the span wise and chord wise directions are straight lines. The trailing vortices start from the span wise divisions of the lifting surface on the upstream end and pass along the chord wise divisions to infinity. Each horseshoe vortex is placed on the associated panel of the lifting surface. As per incompressible, thin airfoil theory, the aerodynamic center of a surface is at the quarter chord (Clancy [20]). Thus, the finite bound vortex is placed along the panel quarter-chord and has the end points on the panel edges. The rest of the horseshoe comprises of two trailing vortices which has an endpoint at the bound vortex and trails off to infinity. Each horseshoe vortex is associated with one lifting panel. In order to model the entire flow field, the horseshoe vortices from all panels are assembled thus forming a vortex lattice. Each panel has a point, called control point at which the flow tangency boundary condition is satisfied. On each panel, it is located at three-quarter length chord-wise and centered between the trailing vortices of adjacent panels. In the matrix, the tangency boundary condition can be written as

$$[C]\{\Gamma\} = \{V\} \tag{3.1}$$

where C is the influence coefficient matrix, Γ is the circulation distribution vector and V is the downwash velocity distribution vector. The reasoning behind the $1/4^{th}$ and $3/4^{th}$ rule for placing the bound vortex and the control point in each panel is presented in Appendix A.

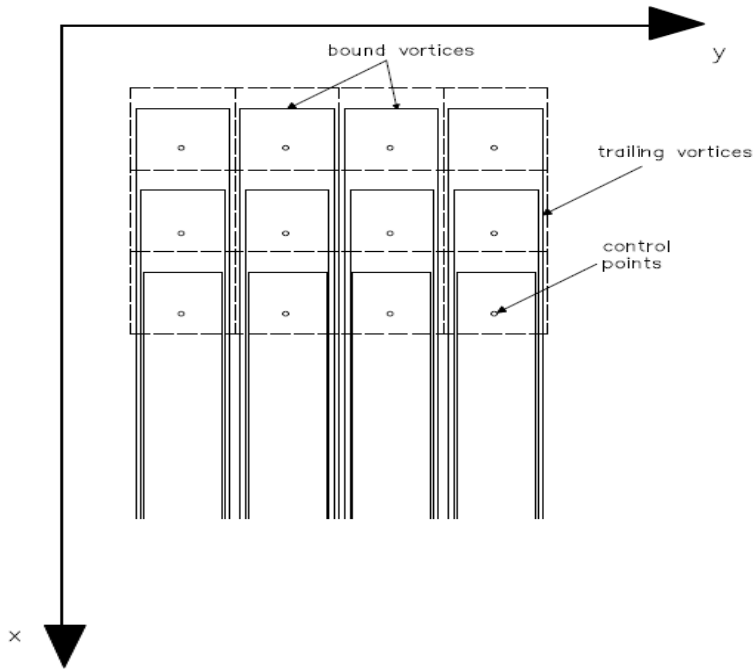

Figure 3.1 Lattice configuration of 3 rows and 3 columns on the wing

For the turbine case, the streamlines are not rectilinear, but helical. To model the turbine in a manner consistent with the vortex lattice method the span wise divisions must follow free streamlines. Using this framework, the span wise divisions are made such that each lies along a line of constant distance from the axis of the turbine rotation. Chord wise divisions are made along lines of constant-percent-chord, similar to that done for the wing analysis. Also for the turbine case, the control points are positioned at the three quarter chord lines or two quarter chord from the bound vortex. Each control point is placed along the mean width span-wise of its panel in order to be properly centered between the filament legs or trailing vortices.

3.2 Description of Flow and Forces of a Turbine Blade

The flow along the turbine is illustrated in Figure 3.2. The lift force on a differential element at radial distance r is denoted as dL, and by definition is normal to the resultant velocity of the blade relative to the fluid and the drag force dD in direction opposite of the resultant blade velocity. The lift and drag force components, resolved in directions parallel and perpendicular to the current are denoted as dT and dH respectively. The dT component represents the drag force of the current. The differential torque dQ is the moment of dH; i.e., dQ= r .dH. As discussed earlier, the influence coefficient matrix C is determined by the blade geometry and the induced velocity vector is determined through the kinematic condition which involves current velocity and blade geometry. A linear matrix equation solved for the circulation vector Γ. Once Γ is known, the desired parameters such as lift and induced drag can be calculated. Next, let us examine the flow characteristics of blade section. The transverse velocity due to rotation is equal to $2\pi nr$. With incoming current velocity represented as V_∞, the resultant velocity of the blade with respect to the fluid is the vector sum of $2\pi nr$ and V_∞. The angle of attack of the blade section is given by

$$\alpha = \beta - \theta \tag{3.2}$$

where θ is the pitch angle and

$$\beta = \tan^{-1} \frac{\overline{V_\infty}}{2\pi nr} \tag{3.3}$$

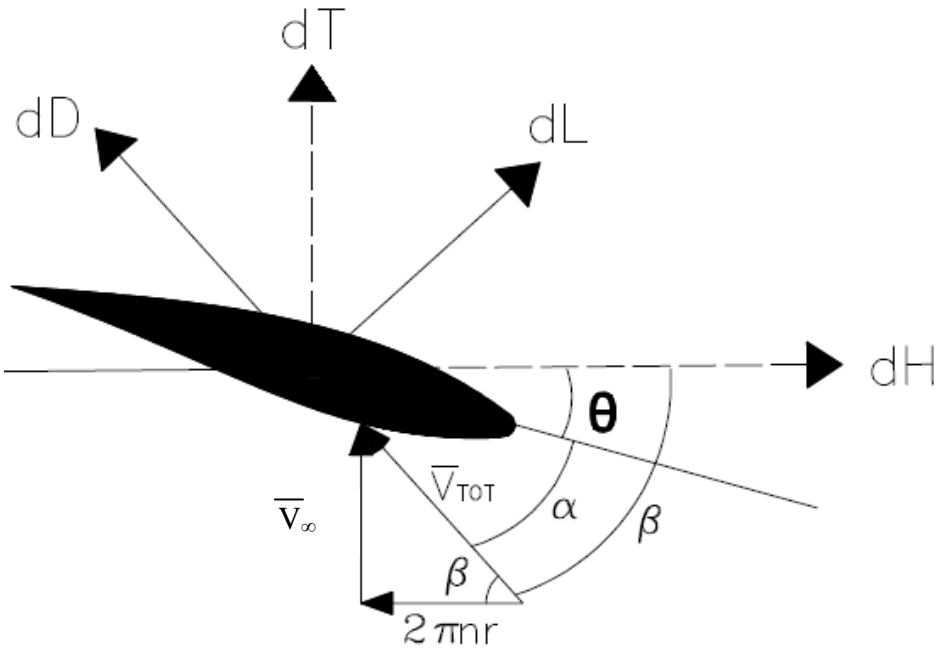

Figure 3.2 Showing the forces acting on the blade

Referring to Figure 3.2, one can note the following relations for the force, moment and power on as differential element:

$$dT = dL\cos\beta + dD\sin\beta \tag{3.4}$$

$$dH = dL\sin\beta - dD\cos\beta \tag{3.5}$$

$$dQ = r.dH = r.(dL\sin\beta - dD\cos\beta) \tag{3.6}$$

$$dP = 2\pi n[dQ] = 2\pi n[r.(dL\sin\beta - dD\cos\beta)] \tag{3.7}$$

By integrating the above, one can determine the total thrust, torque and power:

$$T = \int \left(\frac{dL}{dr}\cos\beta + \frac{dD}{dr}\sin\beta\right) dr$$

$$Q = \int r.\left(\frac{dL}{dr}\sin\beta - \frac{dD}{dr}\cos\beta\right) dr \tag{3.8}$$

$$P = \int 2\pi n\left[r.\left(\frac{dL}{dr}\sin\beta - \frac{dD}{dr}\cos\beta\right)\right] dr$$

3.3 Influence of Coefficient Matrix for Turbine Blade Analysis

The influence coefficient matrix C for the turbine is found by using a procedure similar to that used for the wing. The integration of the Biot-Savart Law is performed using a numerical representation of each vortex filament as a series of discrete line segments.

Figure 3.3 Blade layout of the turbine

In a turbine, the multiple blades on a turbine configuration are arranged symmetrically as shown in the Figure 3.3. In geometric modeling, only the base blade geometry is initially entered. This base blade establishes the locations of the control points and the horseshoe vortices. By symmetry, the locations of the control points and the horseshoe vortices of the remaining blades are established. Similarly, in determining the induced velocity, after performing the summation of integrations over all of the vortex filaments of the base blade, the procedure is repeated with vortex filaments displaced $2\pi/N$ radians (where N is the number of blades). Note that we consider all the blades together in the modeling and simulation, but the symmetry of blades helps to simplify the computation of vortex locations and induced velocities.

3.4 Boundary Condition Vector

The boundary requirements for the turbine problem are the same as those for the wing, in that no flow is allowed to pass through the control points. The components of the boundary condition vector for the turbine are more complex than those of the wing boundary condition vector.

In case of the flat, untwisted wing, the right hand side of Equation 2.37 becomes ($-V_\infty * \alpha$) and this is constant for all panels. For the turbine, V_∞ becomes the local total velocity (V_{TOT}), equal to the vector sum of current velocity and panel rotational velocity. The current direction is normal to the plane of rotation, therefore

$$V_{TOT} = \left[{V_\infty}^2 + (2\pi nr)^2\right]^{1/2} \tag{3.9}$$

This vector points in the direction of the flow seen by the turbine blade as shown in Figure 3.2

Each panel is oriented parallel to this local total velocity vector at the zero local angle of attack condition. Radial distribution of the angle of attack, which depends on the pitch distribution, rotational speed of the blade and current velocity according to the following equations discussed earlier

$$\begin{aligned} \alpha &= \beta - \theta \\ \beta &= \tan^{-1}\frac{\overline{V_\infty}}{2\pi nr} \end{aligned} \tag{3.10}$$

is then specified for each of the panels in the vortex lattice.

3.5 Determination of Circulation Strengths and Other Quantities of Interest

The matrix equation corresponding to the no-flux condition is then solved to determine the span wise and chord wise distribution of circulations in the vortex lattice. Once the circulation distribution along the turbine blade is found, the performance parameters are calculated. Lift force is found using the Kutta-Joukowski theorem (Masquelier [17]):

$$L_n = \left(\rho . b_n . \bar{V}_{TOT,n} X \bar{\Gamma}_n\right) . \bar{n} \tag{3.11}$$

where ρ is the fluid density, b_n is the length of the bound vortex of panel n, and V_{TOT} is the total panel velocity, combining current and rotational velocity of section n. For small angles of attack, the expression for the lift can be written as

$$L_n = \rho . b_n . \left|\bar{V}_{TOT,n}\right| . |\bar{\Gamma}_n| \tag{3.12}$$

and the corresponding lift coefficient as

$$C_{L_n} = \frac{L_n}{{}^1/_2 . \rho . V_{TOT,n}^2 . A_n} \tag{3.13}$$

where, A_n is the area, approximated by the product of panel span and panel chord C_n, the expression for the lift coefficient becomes

$$C_{L_n} = \frac{2 . \Gamma_n}{V_{TOT,n} . c_n} \tag{3.14}$$

The panel pressure (which in actuality is the local pressure difference between the pressure and suction sides) is found by dividing the lifting force by the panel area.

$$Pr_n = \frac{L_n}{A_n} \tag{3.15}$$

The panel pressure is assumed constant throughout each of the panels in the lattice.

Thrust and torque are calculated from the lift force as described earlier. However we cannot compute the viscous drag, because we are considering the flow to be inviscid. The induced drag is given by (Bertin [9])

$$D_n = \rho . V_{TOT,n} . \Gamma_n . b_n . \sin(\alpha_{i,n}) \tag{3.16}$$

where, D_n is the drag of the n^{th} panel and $\alpha_{i,n}$ is the induced angle of attack of the n^{th} panel.

The induced incidence α_i (Bertin [9]) is given by

$$\alpha_i = -\frac{1}{8\pi}\int_0^l \frac{C_L . c}{(y-\eta)^2}\, d\eta \tag{3.17}$$

where, C_L is the lift coefficient, c is the chord, l is the span, y is the point at which induced incidence is calculated and η is point varying along the span.

Power coefficient C_P is found by dividing the rotor power obtained (the product of torque (Q) and omega (2πn)) by the maximum available power.

$$C_P = \frac{2\pi n . Q}{\frac{1}{2}\rho A V_\infty{}^3} \tag{3.18}$$

The above procedure is thus used to determine the performance parameters of a turbine with thin blade sections.

3.6 Special Case: Planar Wing

In the validation study for the algorithm developed in the thesis, we have also considered flow about planar wings. For the special case of a plane wing in a uniform flow field, the procedure to determine lift is described below.

The velocity induced at a point due to the vortex filament segment of strength Γ_n and length dl is described by the Biot-Savart law,

$$\overline{dV} = \frac{\Gamma}{4\pi}\frac{\overline{dL}X\bar{r}}{|\bar{r}|^3} \tag{3.19}$$

where, dV is the incremental velocity vector induced at an arbitrary point due to a vortex filament segment dL; Γ is the strength of the vortex filament segment; and r is the vector whose tail is located at the center of the filament segment, and whose head is located at the control point, the magnitude of the induced velocity is

$$dV = \frac{\Gamma \sin\theta \, dl}{4\pi r^2} \tag{3.20}$$

The velocity induced by a horseshoe vortex composed of three straight filaments segments is described by Equations 2.23 to 2.31. The above approximation is consistent with the assumption of linearized theory. The unknown circulation strengths required to satisfy these boundary conditions are found by solving the system of linear equations developed in the horseshoe vortex section. For a planar wing, $Z_{1n} = Z_{2n} = 0$ for all of the bound vortices. Furthermore, Z = 0 for all of the control points. Note that, for the planar wing, all three components of the horseshoe vortex representing the n^{th} panel induce a velocity downward at the control point of the m^{th} panel expression of which is

$$V_{AB}$$

$$= \frac{\Gamma_n}{4\pi}\left\{\frac{1}{(x-x_{1n})(y-y_{2n})-(x-x_{2n})(y-y_{1n})}\left[\frac{(x_{2n}-x_{1n})(x-x_{1n})+(y_{2n}-y_{1n})(y-y_{1n})}{((x-x_{1n})^2+(y-y_{1n})^2)^{1/2}}\right.\right.$$

$$\left.\left.-\frac{(x_{2n}-x_{1n})(x-x_{2n})+(y_{2n}-y_{1n})(y-y_{2n})}{((x-x_{2n})^2+(y-y_{2n})^2)^{1/2}}\right]\right\}$$

(3.21)

$$V_{A\infty} = \frac{\Gamma_n}{4\pi}\left(+\frac{1}{y_{1n}-y}\left[1+\frac{x-x_{1n}}{((x-x_{1n})^2+(y-y_{1n})^2)^{1/2}}\right]\right) \tag{3.22}$$

$$V_{B\infty} = \frac{\Gamma_n}{4\pi}\left(-\frac{1}{y_{2n}-y}\left[1+\frac{x-x_{2n}}{((x-x_{2n})^2+(y-y_{2n})^2)^{1/2}}\right]\right) \tag{3.23}$$

Thus,

$$V_{m,n} = V_{AB} + V_{A\infty} + V_{B\infty} \tag{3.24}$$

$V_{m,n}$

$$= \frac{\Gamma_n}{4\pi}\left\{\frac{1}{(x-x_{1n})(y-y_{2n})-(x-x_{2n})(y-y_{1n})}\left[\frac{(x_{2n}-x_{1n})(x-x_{1n})+(y_{2n}-y_{1n})(y-y_{1n})}{((x-x_{1n})^2+(y-y_{1n})^2)^{1/2}}\right.\right.$$

$$\left.-\frac{(x_{2n}-x_{1n})(x-x_{2n})+(y_{2n}-y_{1n})(y-y_{2n})}{((x-x_{2n})^2+(y-y_{2n})^2)^{1/2}}\right]$$

$$\left.+\frac{1}{y_{1n}-y}\left[1+\frac{x-x_{1n}}{((x-x_{1n})^2+(y-y_{1n})^2)^{1/2}}\right]-\frac{1}{y_{2n}-y}\left[1+\frac{x-x_{2n}}{((x-x_{2n})^2+(y-y_{2n})^2)^{1/2}}\right]\right\}$$

(3.25)

Summing the contributions of all the vortices to the downwash at the control point of the mth panel:

$$V_m = \sum_{n=1}^{N} V_{m,n} = C_{m,n} \,.\, \Gamma_n \tag{3.26}$$

The free stream velocity component normal to the wing is $V_\infty \sin \alpha$ at any point on the wing. If the total downwash induced velocity of the horseshoe vortex at the control point cancels the normal component of the free stream velocity than, the resultant flow will be tangential to the wing.

i.e.,

$$V_m + V_\infty sin\alpha = 0 \tag{3.27}$$

Thus from the above two equations we obtain

$$C_{m,n}.\Gamma_n = -V_\infty \sin\alpha \tag{3.28}$$

Using the VLM code Γ and other quantities of interest are calculated by solving the above matrix equation.

3.7 Onset Flow at the Turbine

In the vortex lattice method, one specifies the onset flow on the blade panels which would be different from the upstream far-field (ie., free stream) current velocity because of the pressure variations along the axial direction and vortices trailing in the swirling wake. The onset velocity on the blade can be different from the free-stream velocity not only in magnitude but also in direction, as illustrated in the figure B.1. To determine the velocity at the turbine we employ an approach suggested in Manwell et al [7] which use the classical blade-element and momentum theories for turbine flows. This involves iterative determination of induction factors that correct for the magnitude and direction of the flow incident right on the turbine blades. This methodology is explained in Appendix B. In methods based on the discretization of the entire flow field, one could specify the current velocity at the upstream open boundary, but in the present surface integral formulation such as VLM only the treatment of the sort used above is possible.

3.8 Trailing Helical Vortices

In the case of a propeller or a turbine, the vortices trailing the blades will align on a helical surface that depends on the blade pitch and the axial and rotational velocities of the turbine blades. Following Masquelier [17], who had carried out the analysis for a propeller, we obtained expressions for the velocity induced by trailing helical line vortices as discussed below.

The wake model described here determines the induced velocities at the blades due to the wake. This induced velocity, combined with current speed and rotational motion, determine the velocity and angle of attack seen by the blades. The induced velocity by a vortex filament at any point in the space is determined using the Biot-Savart Law.

In this appendix, the velocity induced by a single semi-infinite trailing vortex segment of a helical wake is discussed. As shown in the Figure 3.4 Consider two points m and n in the reference frame of rotating disk as (r_m, θ_m, z_m) and (r_n, θ_n, z_n). Let dl be the differential vortex element which will induce a velocity dW at point m, with the position vector R being from m to dl.

By Biot-Savart Law [10], the induced velocity at m due to vortex filament dl is given by

$$d\vec{W}_m = \frac{\Gamma}{4\pi} \frac{\vec{dl} \times \vec{R}}{\left|\vec{R}\right|^3} \tag{3.29}$$

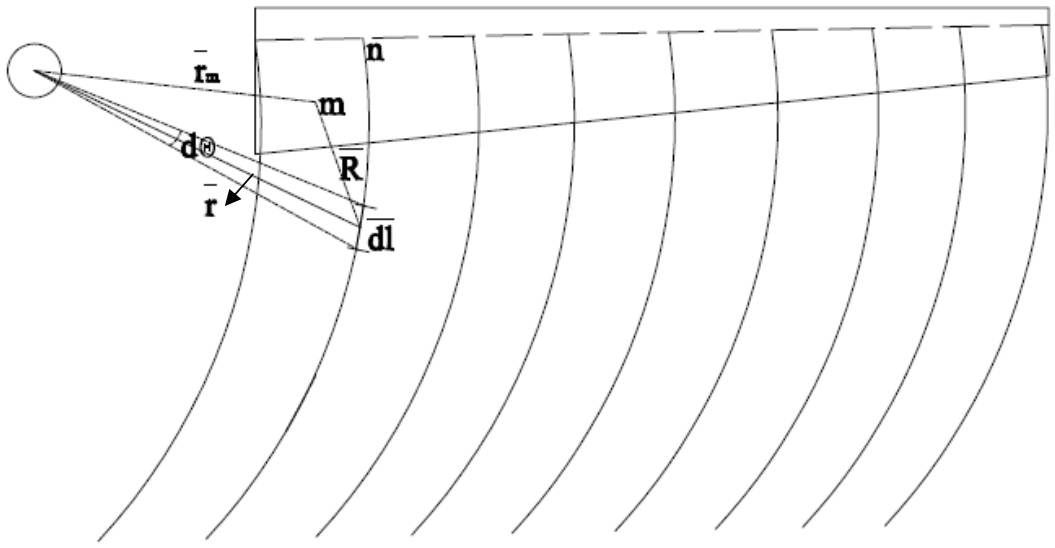

Figure 3.4 Showing the shedding of trailing vortices and the nomenclature.

In the above, n denotes the point on the surface of the blade which emits a helical vortex filament trajectory of which given by

$$X = -k\theta, Y = r_n \sin\theta\,, Z = r_n \cos\theta$$

where k denotes the horizontal distance traversed by trailing vortex lines per unit angle which for a turbine in a current can be shown to be k = r[tan θ_p + (TSR*)$^{-1}$] where θp here denotes the local pitch angle, r the radius of the vortex panel and TSR* (= TSR.r/R) the tip speed ratio. In the above, the TSR term represents the convection of the vortex by the current and tan θp that by the blade pitch.

The velocity induced at point m by a segment dl of the helical filament can be re-written as

$$d\vec{W}_m = \frac{\Gamma}{4\pi} \frac{\vec{dl} \times (\vec{r}_m - \vec{r})}{|(\vec{r}_m - \vec{r})|^3} \qquad (3.30)$$

where r is the vector from origin to dl, r_m is the vector from the origin, which is located at the centre of shaft to point m, Γ_n is the circulation strength in dl. In Cartesian coordinates, above can be written as

$$\begin{gathered}\overrightarrow{dl} = -kd\theta\hat{\imath} + r_n\cos\theta\, d\theta\hat{\jmath} - r_n\sin\theta\, d\theta\hat{k} \\ \bar{r}_m = X_m\hat{\imath} + Y_m\hat{\jmath} + Z_m\hat{k} \\ \vec{r} = X\hat{\imath} + Y\hat{\jmath} + Z\hat{k} = -k\theta\hat{\imath} + r_n\sin\theta\,\hat{\jmath} + r_n\cos\theta\,\hat{k}\end{gathered} \tag{3.31}$$

Substituting equations 3.31 in 3.30 we get,

$$d\overrightarrow{W_m} = \frac{\Gamma}{4\pi}\frac{[-kd\theta\hat{\imath}+r_n\cos\theta d\theta\hat{\jmath}-r_n\sin\theta d\theta\hat{k}]\times[(X_m-X)\hat{\imath}+(Y_m-Y)\hat{\jmath}+(Z_m-Z)\hat{k}]}{[(X_m-X)^2+(Y_m-Y)^2+(Z_m-Z)^2]^{\frac{3}{2}}} \tag{3.32}$$

Performing the cross product and further simplifying we get,

$$\begin{aligned}d\overrightarrow{W_m} &= \frac{\Gamma}{4\pi}\left\{\frac{\hat{\imath}[r_n\cos\theta(Z_m-Z)+r_n\sin\theta\,(Y_m-Y)]}{[(X_m-X)^2+(Y_m-Y)^2+(Z_m-Z)^2]^{\frac{3}{2}}}\right. \\ &+\frac{\hat{\jmath}[k\theta(Z_m-Z)-r_n\sin\theta(X_m-X)]}{[(X_m-X)^2+(Y_m-Y)^2+(Z_m-Z)^2]^{\frac{3}{2}}} \\ &\left.+\frac{\hat{k}[-k\theta(Y_m-Y)-r_n\cos\theta\,(X_m-X)]}{[(X_m-X)^2+(Y_m-Y)^2+(Z_m-Z)^2]^{\frac{3}{2}}}\right\}d\theta\end{aligned} \tag{3.33}$$

The above expression represents the velocity induced at point m due to dl. Upon integration, one obtains the following expression for the total velocity induced at m by trailing helical vortex starting at n:

$$\vec{W}_m$$

$$= \frac{\Gamma}{4\pi}\int_{-\infty}^{0}\left\{\frac{\hat{\imath}[r_n\cos\theta(Z_m - r_n\cos\theta) + r_n\sin\theta\,(Y_m - r_n\sin\theta)]}{[(X_m + K\theta)^2 + (Y_m - r_n\sin\theta)^2 + (Z_m - r_n\cos\theta)^2]^{\frac{3}{2}}}\right.$$

$$+\frac{\hat{\jmath}[k\theta(Z_m - r_n\cos\theta) - r_n\sin\theta(X_m + K\theta)]}{[(X_m + K\theta)^2 + (Y_m - r_n\sin\theta)^2 + (Z_m - r_n\cos\theta)^2]^{\frac{3}{2}}} \qquad (3.34)$$

$$\left.+\frac{\hat{k}[-k\theta(Y_m - Y) - r_n\cos\theta\,(X_m + K\theta)]}{[(X_m + K\theta)^2 + (Y_m - r_n\sin\theta)^2 + (Z_m - r_n\cos\theta)^2]^{\frac{3}{2}}}\right\}d\theta$$

In the present thesis, θ is taken to span -12π to 0 instead of -∞ to 0 because the effect decays rapidly with distance. Using the above equation the velocity induced W by vortices trailing all the panels are computed.

In this chapter, we presented the vortex lattice method (VLM) and the algorithms based on the VLM to analyze flow about plane wings and turbines. The codes developed are first validated as discussed in the next chapter.

CHAPTER 4

VALIDATION STUDY

The vortex lattice method algorithm developed in the thesis is first validated by considering the following cases

- Flow about an inclined flat plate
- Flow about a finite aspect ratio flat plate and comparison with Prandtl's Lifting-Line theoretical result
- Flow about a Swept Wing

and comparing the computed results with respective theoretical or other published results.

4.1 Flow about a Flat Plate

From thin airfoil theory, we know that the lift coefficient for flat plates with small angle of attack is given by (Newman [13]).

$$C_L = 2\pi\alpha \qquad '\alpha' \, is \, in \, radians$$

$$C_L = 0.11\alpha \qquad '\alpha' \, is \, in \, degress$$

$$\frac{\Delta C_L}{\Delta \alpha} = 0.11$$

As validation, flow about a flat plate is simulated using the vortex lattice method and the VLM results compared with the above theoretical result. In the VLM simulation, the plate dimensions and flow parameters are taken to be

Length, L = 5 m

Width, B = 0.1 m

Aspect Ratio = L/B = 50

ρ = 1000 kg/m^3

V_∞ = 1 m/sec

$\alpha = 2^0$ to 12^0

Panel Size = 30 X 30

The results and comparisons are summarized in the following Figure 4.1 and Table 4.1

Alpha (α) in degrees	VLM code computed CL	Theoretical CL	Error in Percentage (%)
2	0.2078	0.22	5.871029836
4	0.4154	0.44	5.922002889
6	0.6225	0.66	6.024096386
8	0.8289	0.88	6.164796719
10	1.0342	1.1	6.362405724
12	1.2382	1.32	6.606364077

Table 4.1 shows the C_L values calculated using VLM code and theoretical equation for an aspect ratio of 50

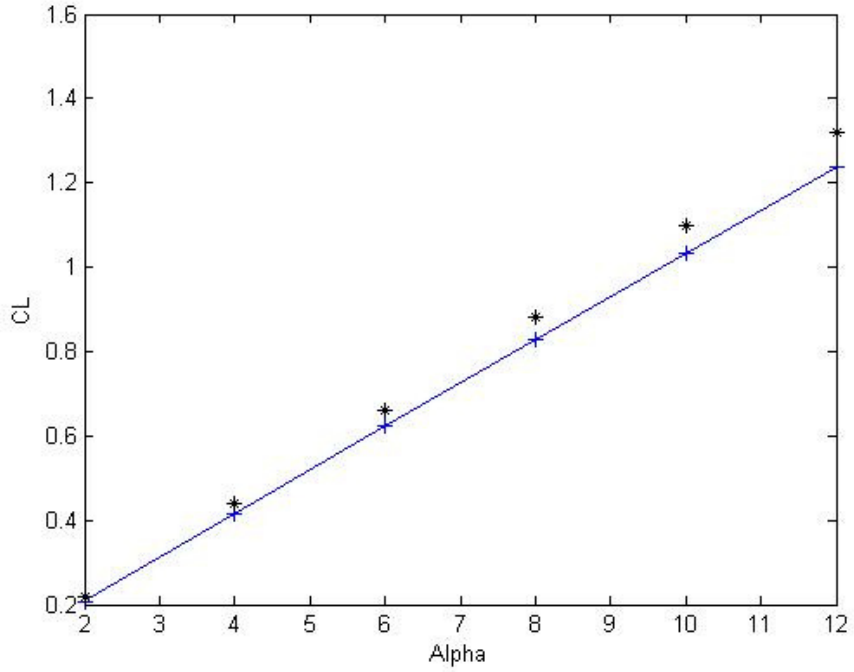

Figure 4.1 The solid line represents VLM results from the code. The asterisk marks are calculated from the theoretical lift coefficient equation.

As can be noted, the agreement between the VLM results and the theory is excellent in particular at small angle of attack which is to be expected because the linear inviscid air-foil theory is more accurate at smaller angles of attack.

4.2 Comparisons with Prandtl's Lifting Line 3D Theory

Next, VLM computations are carried out for the lift coefficient C_L of finite-aspect ratio wing and comparing with Prandtl's lifting line theoretical results (Bertin [9], Anderson [11]). Here the length (span wise) is taken to be 10m and the width (chord wise) is varying with respect to aspect ratio, ranging from 0 to 20. The angle of attack is taken as 6^0. The plate is discretized with one panel chord wise and 5 panels span wise. As can be observed from Figure 4.2, the agreement between the VLM and the lifting-line theory is

quite excellent. However the results obtained with 5 panels span wise and 5 panels chord wise show larger difference (Figure 4.3), because the lifting-line theory which uses only one bound vortex is more closer to VLM modeling with one chord wise panel.

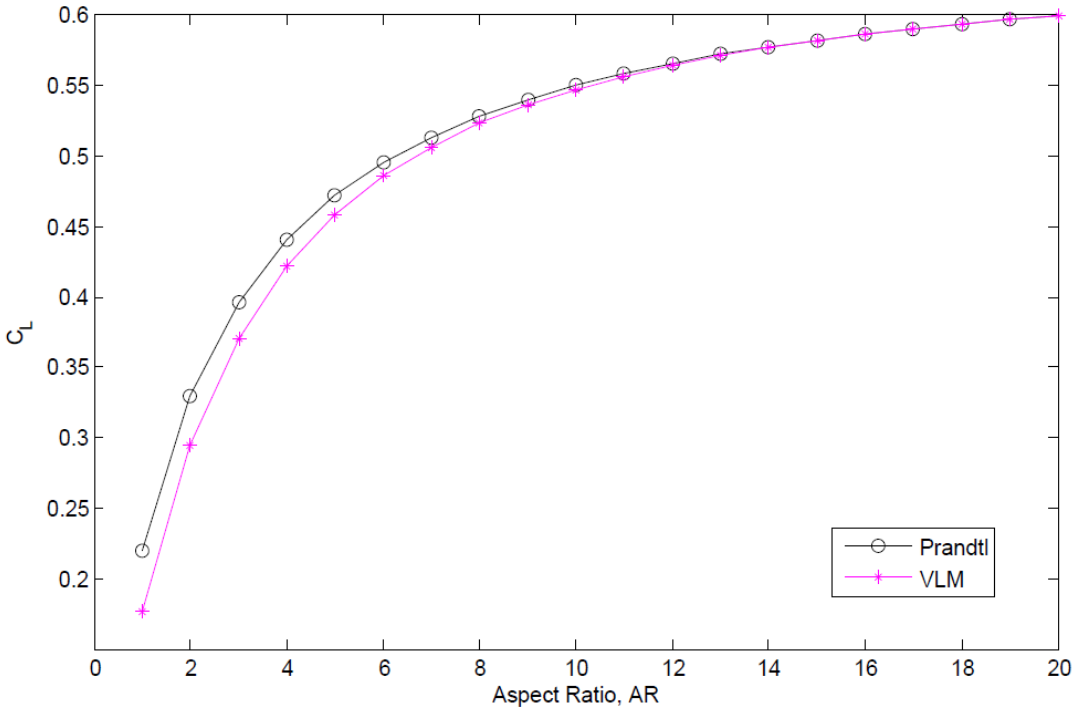

Figure 4.2 Prandtl's lifting line and VLM aspect ratio theory comparison with VLM using (5x1) panels.

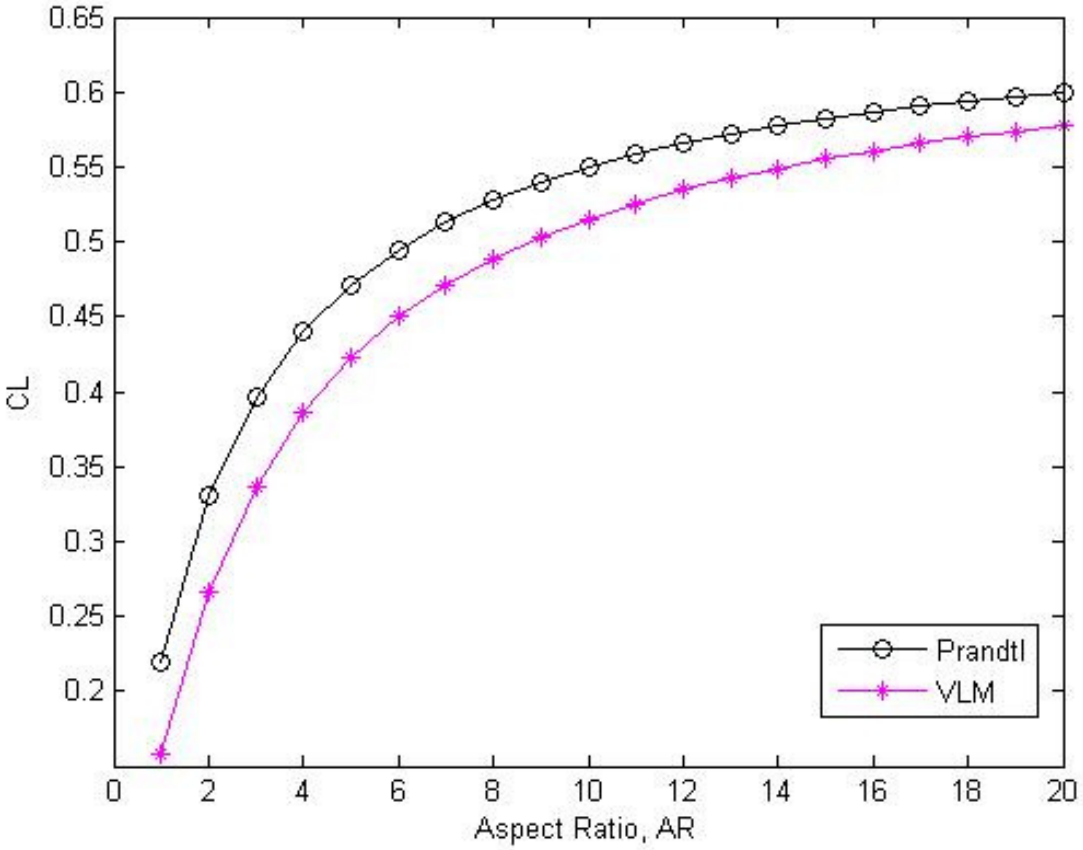

Figure 4.3 Prandtl's lifting line and VLM aspect ratio theory comparison with VLM using (5x5) panels.

4.3 Flow past a Swept Wing

Another case considered for validation is analysis of flow past a swept, planar, uncambered wing with an aspect ratio of five and a swept angle of 45^0, as illustrated in Figure 4.4. The same problem has been analyzed using the VLM in Bertin [9]. Experimental measurements have also been made for this problem by Weber, et al., [15]. The flow field under consideration is symmetric with respect to the X-Z plane. As shown in Figure 4.3, the plan form of the wing is discretized with 8 panels symmetrically distributed over the y-axis of the wing, i.e., 4 on the starboard side and the other 4 on port side. Each panel spans the entire chord. The trailing vortices are parallel to the x-axis.

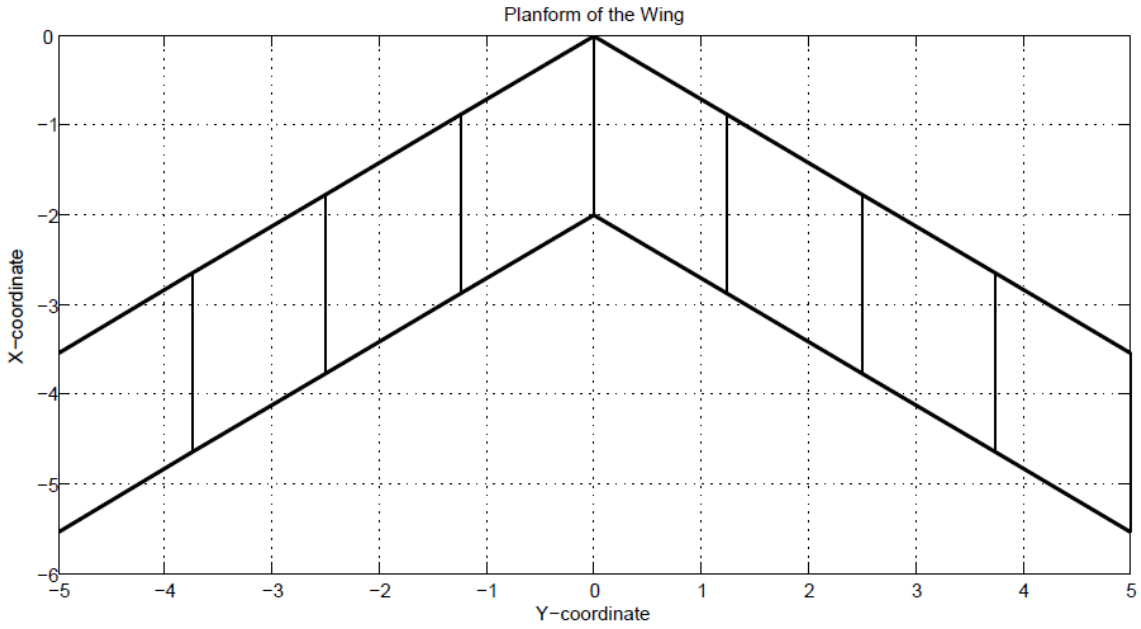

Figure 4.4 Panel layout of the wing

The lift curve generated using the present VLM is compared, in Figure 4.5, with experimental results reported in Weber, et al., [15]. The experimentally determined values of lift coefficient are for a wing of constant chord and of constant section which is swept 45 degrees. The slope of a lift curve computed by Bertin [9] equals 0.0601 per degree, while the slope of a lift curve calculated by the present VLM code is 0.0601 per degree. The error is 0%; in other words, our VLM results exactly match with the VLM results obtained in Bertin [9]. Also note that the VLM code calculated lift coefficients are in good agreement with the experimental values, in particular at low angles of attack. The discrepancy at large angle attack is perhaps due to viscous effect not captured in the VLM.

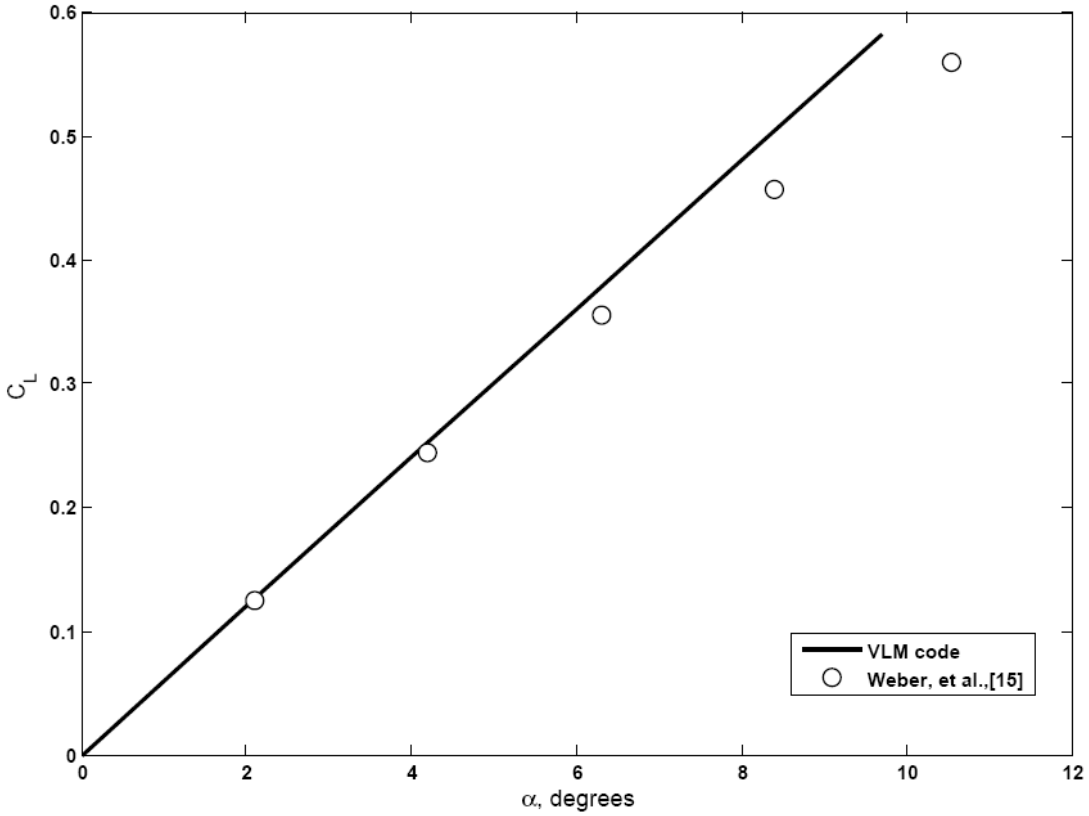

Figure 4.5 The circular rings are the experimental data from Weber, et al., [15]. The solid line represents the lift coefficients calculated from the present VLM code.

The validation study carried out in this chapter demonstrates that out VLM code is accurate and hence can be applied to the study of turbine flow.

CHAPTER 5

VLM RESULTS FOR TURBINE FLOW

We have simulated flow about ocean current turbines for a range of flow and geometric parameter values. Most of the results presented correspond to the prototype turbine developed at the COET of the Florida Atlantic University [6]. A simulation of another turbine, for which experimental results are published, is also carried out to assess the performance of the VLM algorithm.

5.1 VLM Analysis of a Turbine Designed for Alderney Race in Channel Islands

In Bahaj et al. [21], experiments were carried out to assess the performance of a marine current turbine designed for operation in the Race of Alderney in the Channel Islands. The experiments results were carried out in a cavitation tunnel for five hub pitch angles ranging from 15^{o} to 30^{0} and tunnel speeds ranging from 0.8 to 2.0 m/s. The turbine model and experimental set up is shown in Figure 5.1. Using the VLM code developed in the thesis, we numerically studied the performance of the turbine and made comparison of the results. The results corresponding to the case of hub pitch angle of 20^{o} and current velocity of 1.73 m/s is shown in Figure 5.2 and that for hub pitch angle of 25^{o} in Figure 5.3. The difference in the computed and experimental results ranges between 10% and 25% depending on the TSR. The difference could be due to several reasons such as (i) the VLM model works well for thin foils while the turbine blades used in the experiment are not thin enough for the thin foil theory to be fully valid, (ii) errors in the experimental measurements and (iii) viscous effects not considered in the VLM model. Results obtained from a full turbulent flow CFD analysis, as currently being carried out in related projects (example Reza [12]) of the COET, could perhaps predict results that better compares with experimental results.

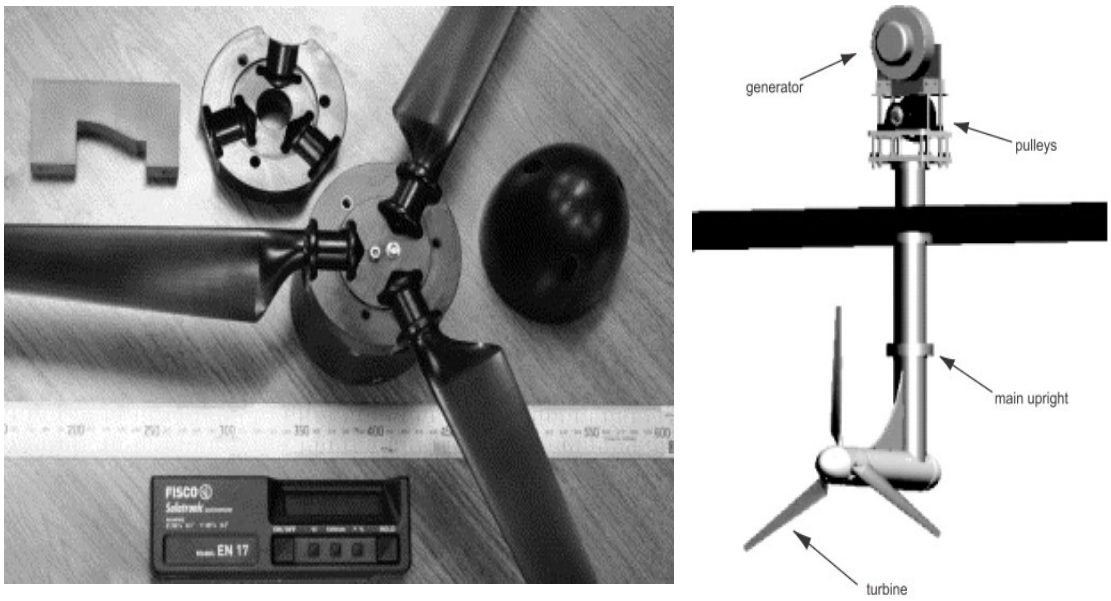

Figure 5.1 Scale model of the turbine studied in the experimental work of Bahaj et al. [21]

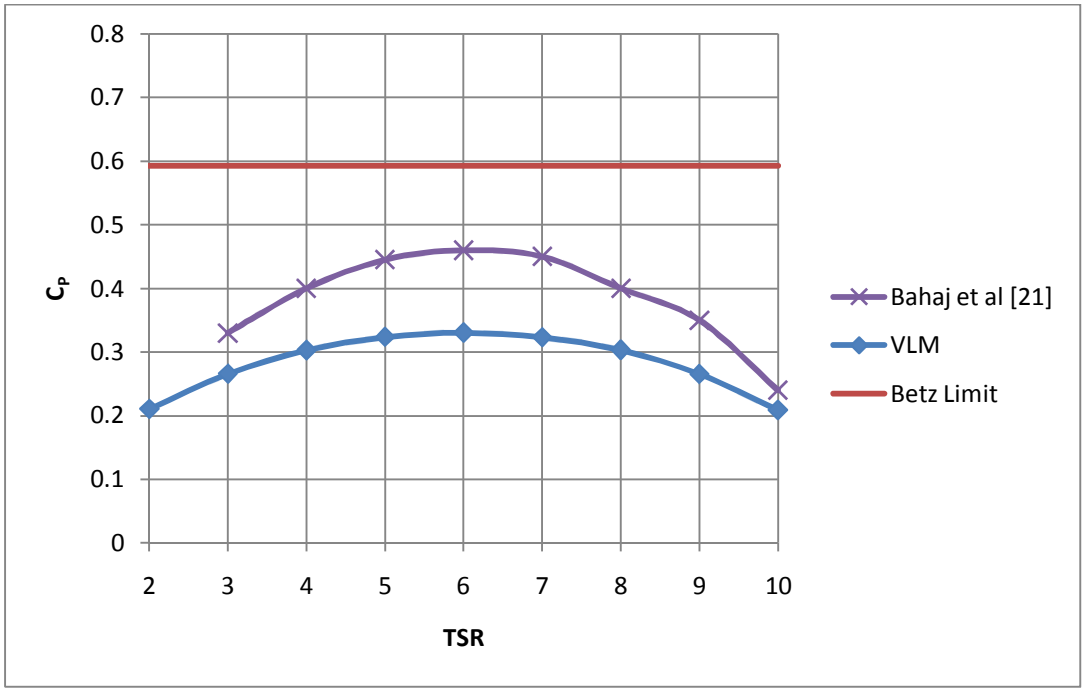

Figure 5.2 Present VLM results compared to experimental results of Bahaj et al. [21] for the case of hub pitch angle 20^o

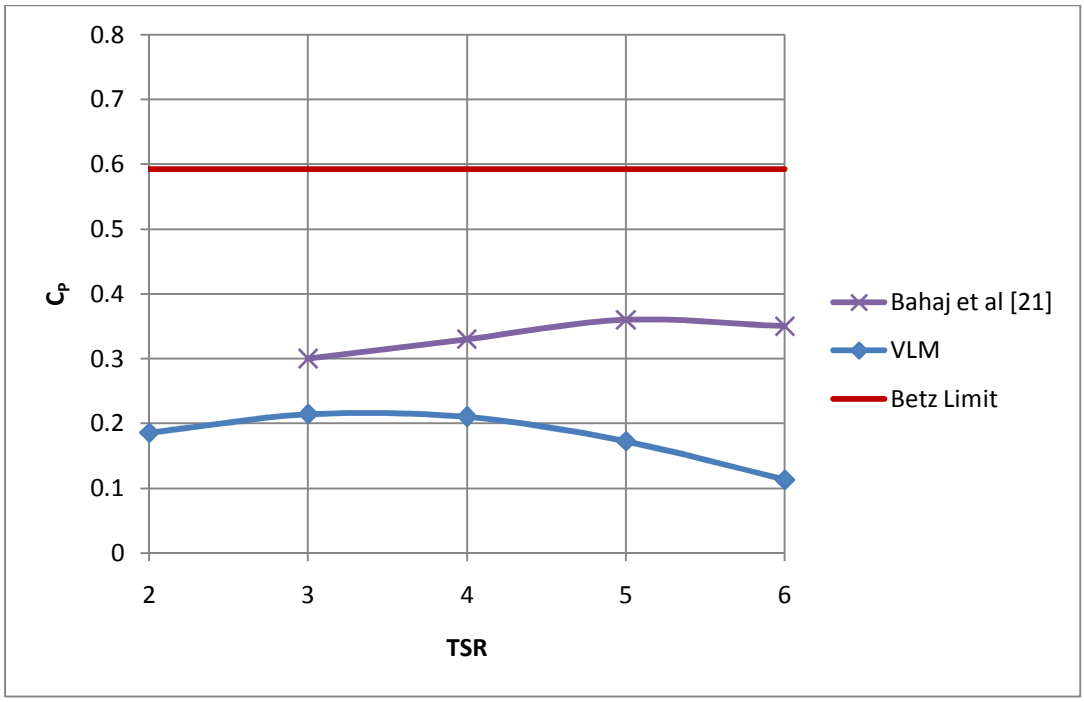

Figure 5.3 Present VLM results compared to experimental results of Bahaj et al. [21] for the case of hub pitch angle 25°

5.2 Simulation of Gulf Stream COET Turbine

In this section, results obtained for the COET turbine are presented. All the results presented correspond to a current velocity of 1.73 m/s which is what is normally observed in the Gulf Stream. The results corresponding to uniform pitch distribution (along the radius) is considered first. Five pitch angle values ($\theta = 0, 2, 4, 6, 8$ degrees) are considered. The power and thrust coefficients Cp and C_T for a range of the tip-speed ratios (TSR) and above pitch angles are presented in Figures 5.4 and 5.5. As can be observed, at a fixed TSR, the power coefficient decreases with increase of θ which is to be expected since the angle of attack decreases with θ (recall, $\alpha = \beta - \theta$ and for a particular TSR β will be constant). The trend of the thrust coefficient is also similar to

that of the power coefficient. However, for a give pitch and TSR, the magnitude of C_T is large than of Cp as to be expected. In the case of propeller, the ratio Ct/Cp represents efficiency. One may take the reciprocal Cp / C_T to be a measure of turbine efficiency which is plotted in Figure 5.6. One finds this ratio to increase with increase of θ. Typical radial variation of the local angle of attack for a range of TSR values, corresponding to a uniform pitch angle of 6^o, is presented in Figure 5.7. One can observe that the angle of attack increases with radius at the hub, reaches a maximum at around 35% of the blade radius, and then decreases along the radius. The distribution of the lift coefficient along the radius for the above case is given in Figure 5.8. Here one observes the maximum C_L decreases with the radius which is also due to the fact that the coefficient is normalized in terms of local velocity magnitude which includes the transverse component of velocity Ωr which increases with the radius. The dimensional lift for the same case is shown in Figure 5.9; here one observes the loading to be elliptic on the blades.

The variation of the total lift coefficient and drag coefficient with respect pitch angle θ for a range of TSR is given in Figures 5.10 and 5.11, respectively. We observe the coefficients to decrease with increasing θ, because of α decreasing with increase of θ. We also note these coefficients to increase with decreasing TSR. The magnitude of the drag coefficient is much smaller than the lift coefficient, as to be expected. The graph of torque coefficient versus TSR for a range of uniform θ is given in Figure 5.12. The general trend is for Cq to decrease with increasing of both θ and TSR. Note that Cq is nothing but Cp/TSR.

Next, results for the COET prototype turbine corresponding to varying pitch angles along the radius are presented. A typical radial variation of the pitch angle of the COET turbine

is shown in Figure 5.13 [22]. The power and thrust coefficients computed for a range of varying pitch angles and TSR are given in Figures 5.14 and 5.15 The general trend is again the decrease of the power coefficients with the increase of the pitch angle. The radial variation of the angle of attack α for the case of hub pitch angle 20^o is given in Figure 5.16. As observed earlier, the maximum angle of attack occurs between r/R=0.35 and 0.45. The radial variation of the lift coefficient for the above case is given in Figure 5.17. Here again, as observed in the case of uniform pitch distribution along the radius, the lift coefficient decreases with the radius with a minimum occurring at around r/R = 0.35.

The power generated by COET blade is provided in Table 5.1. The maximum power generated by the COET blade is 41.3 KW at TSR 8 for a uniform pitch angle $\theta = 2^0$.

Based on the results presented, one could draw some overall conclusions as follows:

1. The TSR corresponding to the maximum power coefficient Cp depends on the pitch angle of the blade, with the TSR corresponding to the maximum Cp decreasing with increase of the pitch angle.
2. For a given TSR, the power coefficient decreases with increase of the pitch angle.
3. The maximum local angle of attack, for the COET turbine, occurs at around r/R=0.35
4. The lift coefficient, normalized with respect to local blade velocity, of the COET turbine decreases with the radius as to be expected.
5. The variation of the pitch (twist) angle along the radius could significantly affect the power coefficient.

With the present VLM tool, which is computationally less demanding and yet can provide accurate results, one could investigate a large family of blade geometries and inflow conditions and obtain an optimum design.

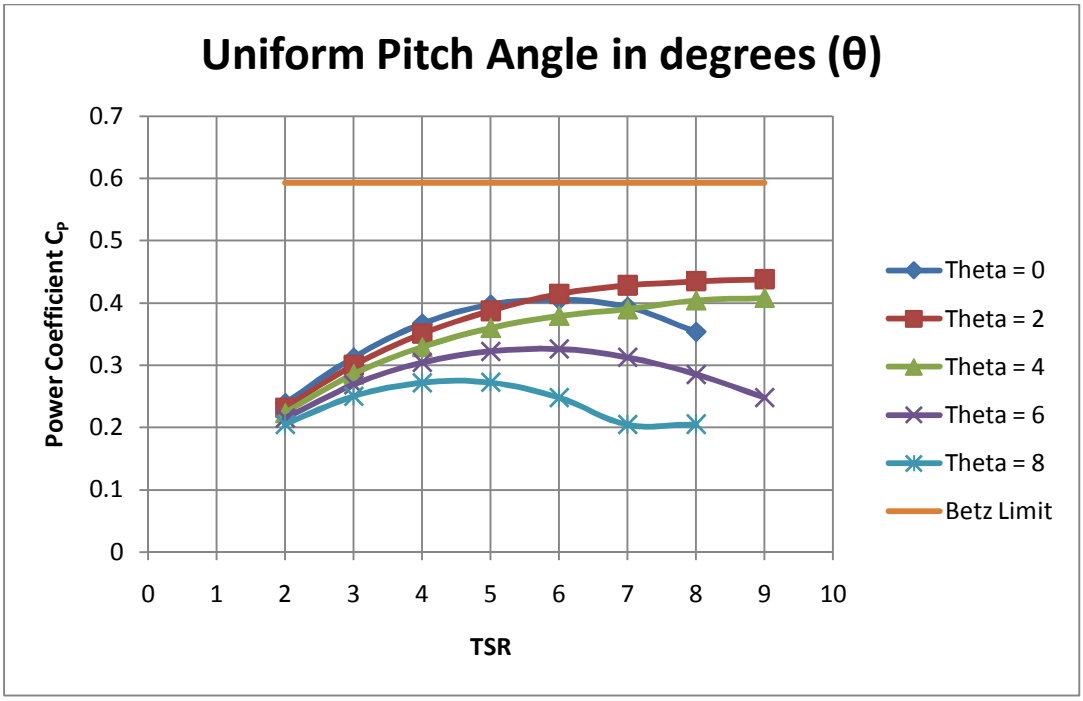

Figure 5.4 VLM results of power coefficients for a range of pitch angles for COET turbine

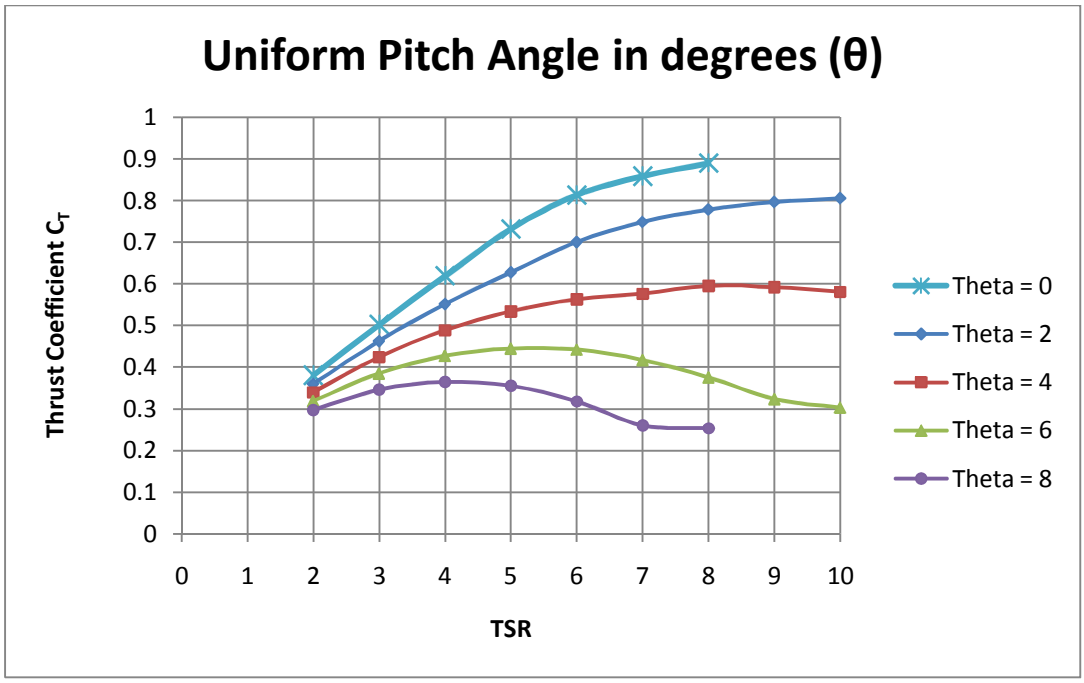

Figure 5.5 VLM results of C_T for a range of pitch angles and TSR for the COET ocean current turbine

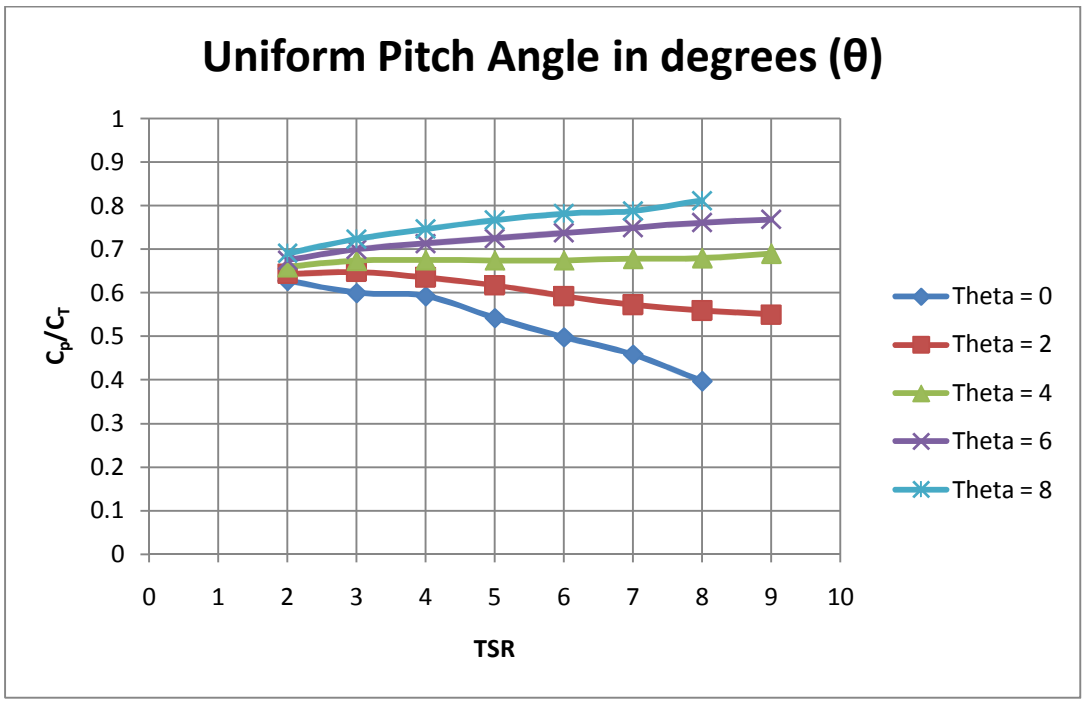

Figure 5.6 VLM results of Cp/Ct for a range of pitch angles and TSR for the COET ocean current turbine

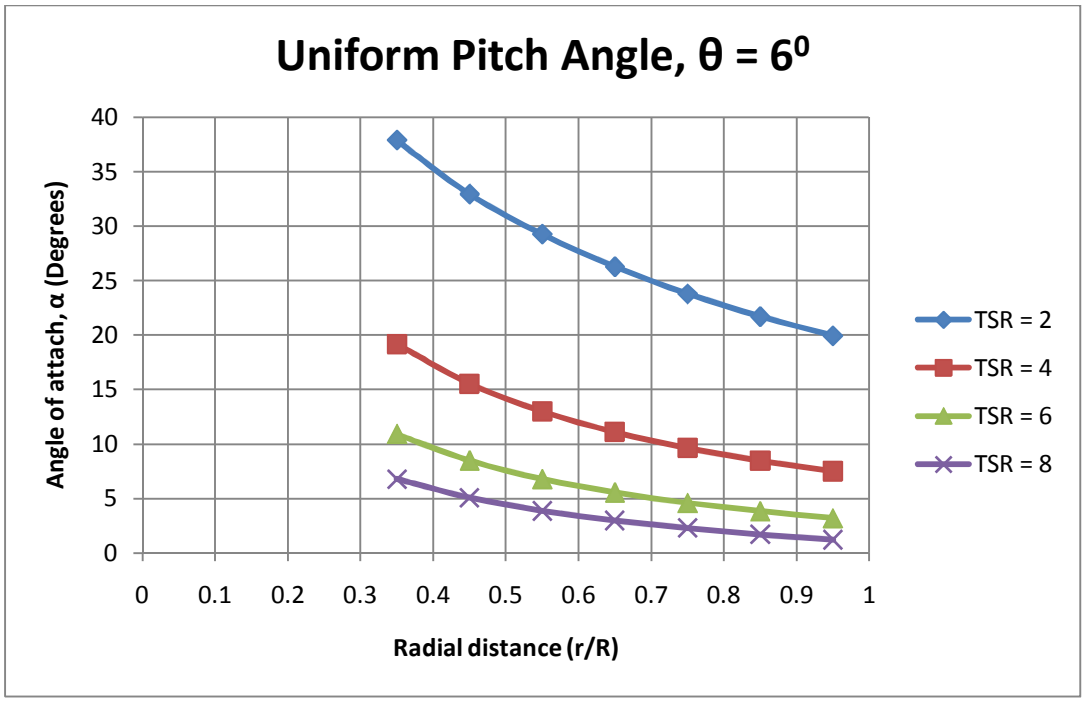

Figure 5.7 Radial variation of the angle of attack for a range of TSR with $\theta = 6^0$

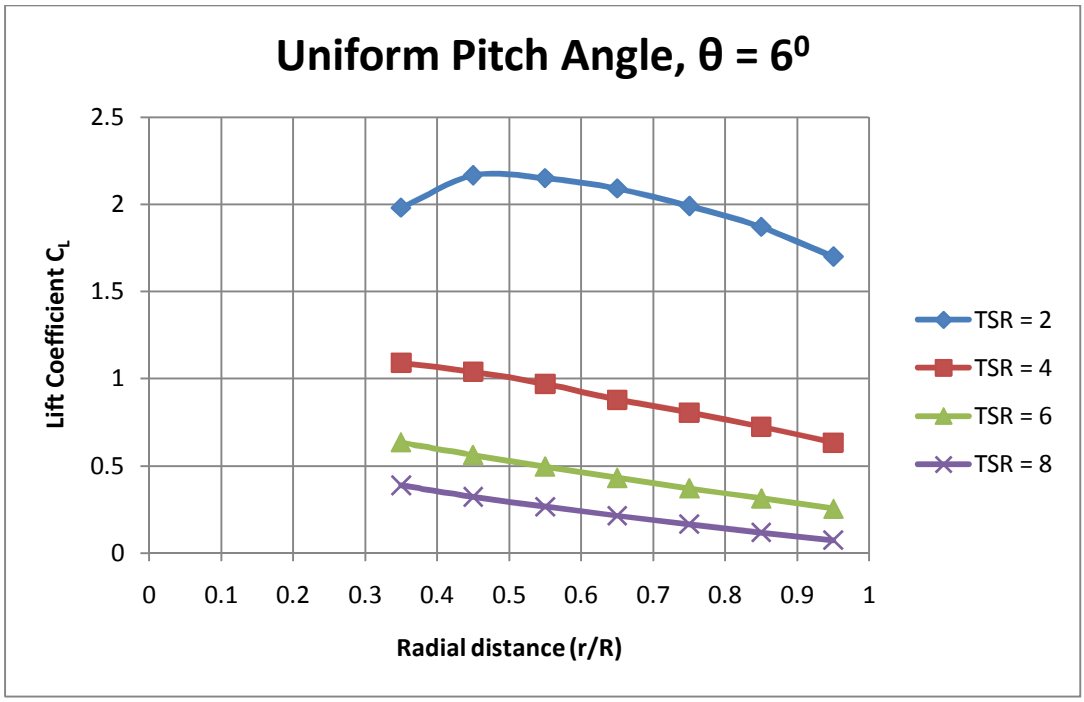

Figure 5.8 Radial variation of lift coefficient for a range of TSR with $\theta = 6^0$

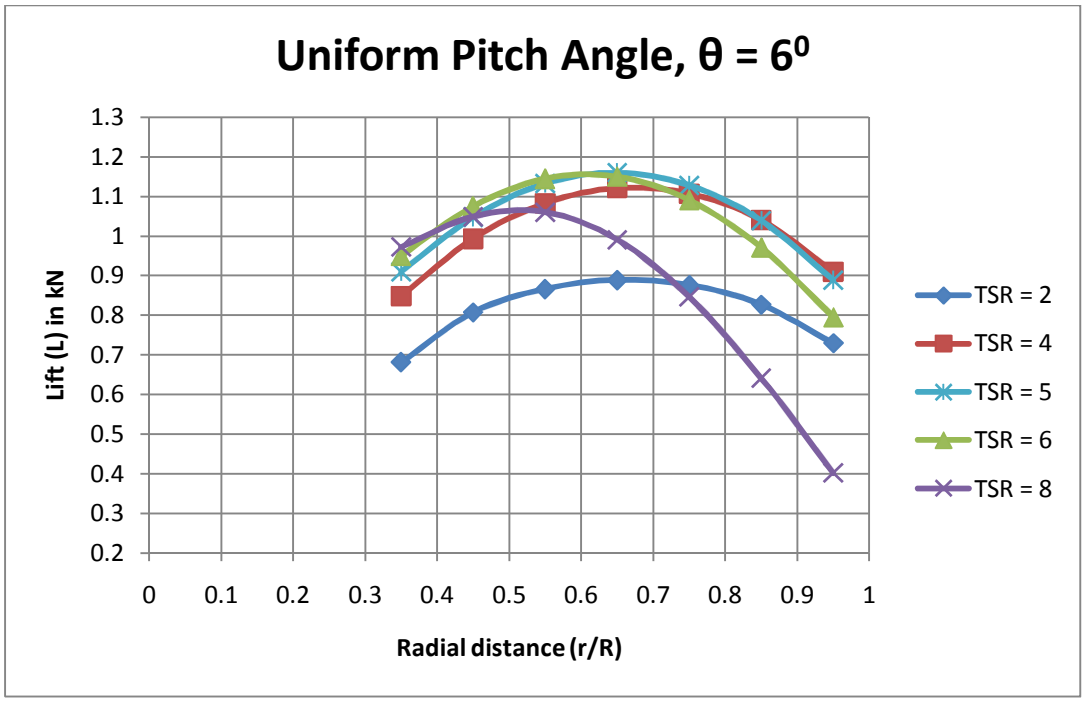

Figure 5.9 Radial variation of dimensional lift for a range of TSR with $\theta = 6^0$

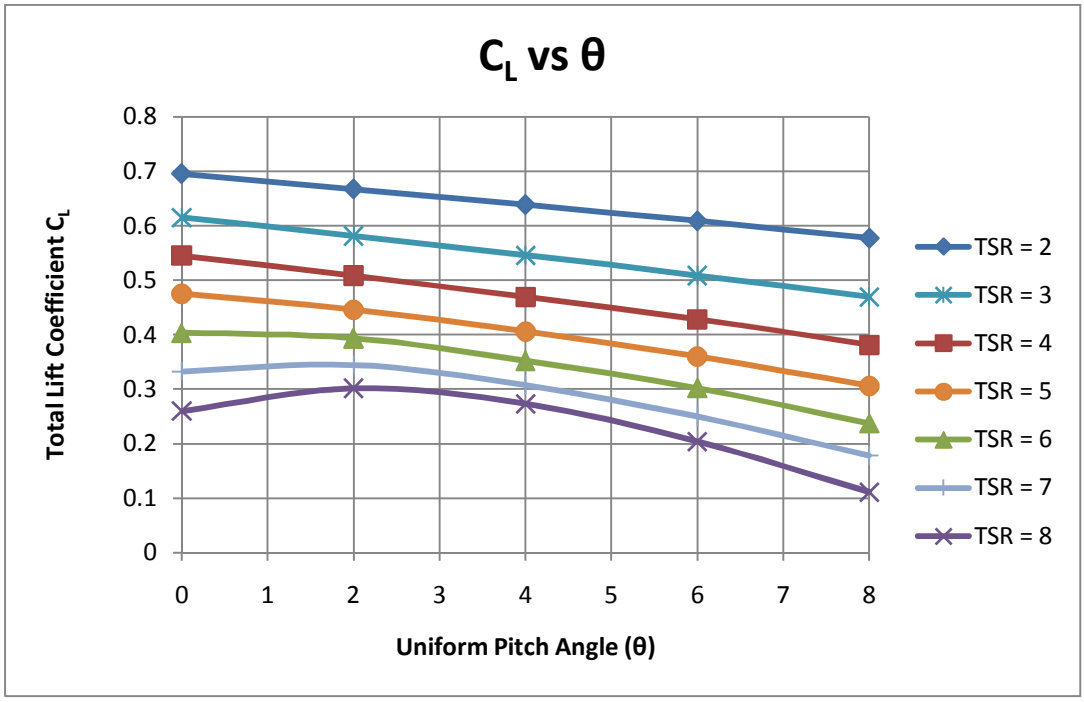

Figure 5.10 Total lift coefficient versus uniform θ for a range of TSR

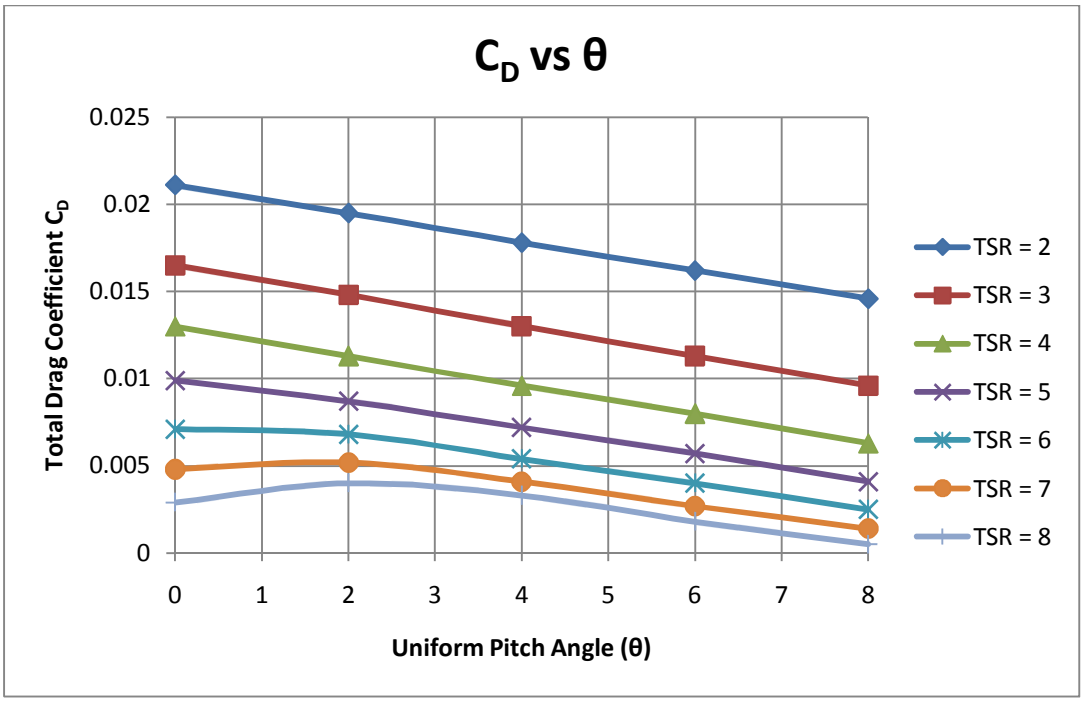

Figure 5.11 Total drag coefficient versus uniform θ for a range of TSR

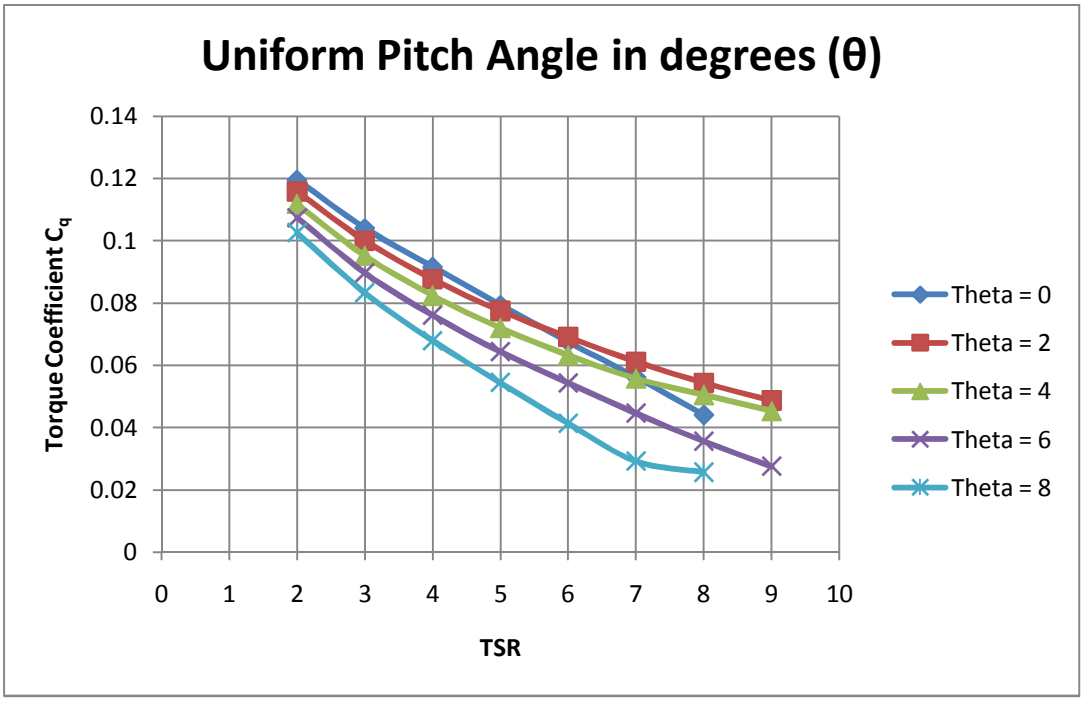

Figure 5.12 Total torque coefficient versus TSR for a range of uniform θ

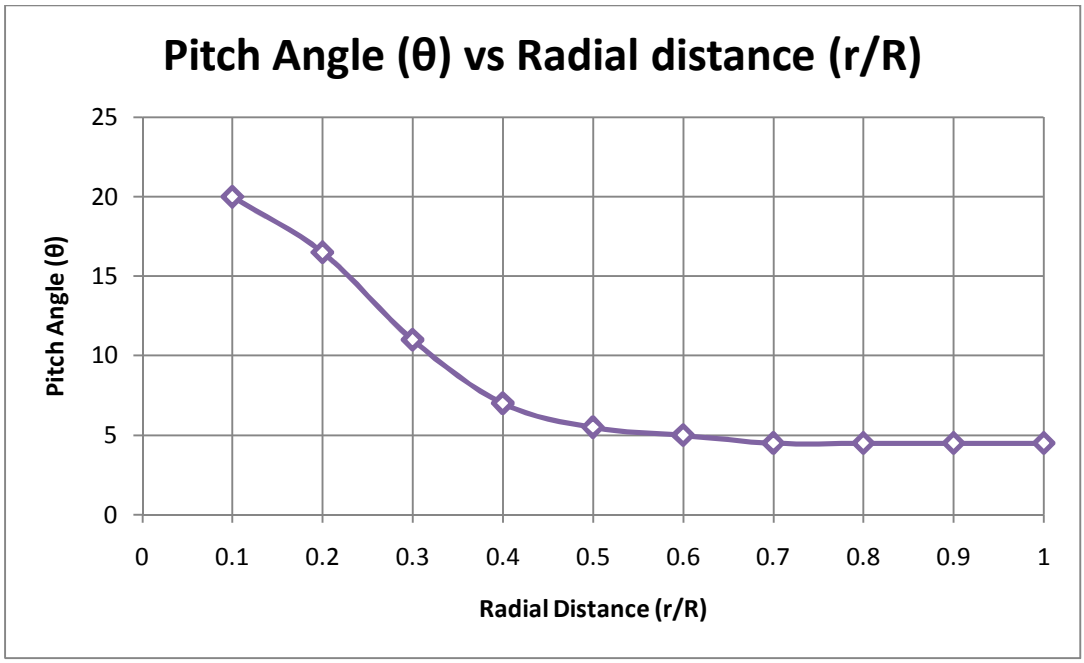

Figure 5.13 Radial variation of the pitch angle for the COET blade

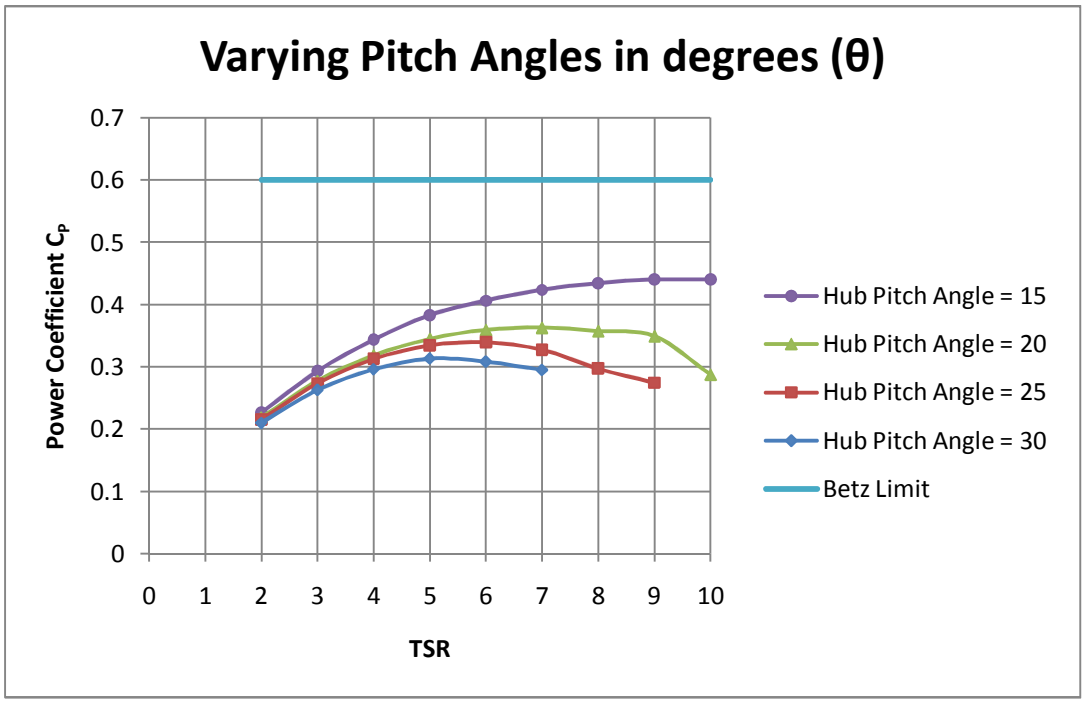

Figure 5.14 Power coefficients computed for a range of varying pitch angles and TSR for the COET ocean current turbine

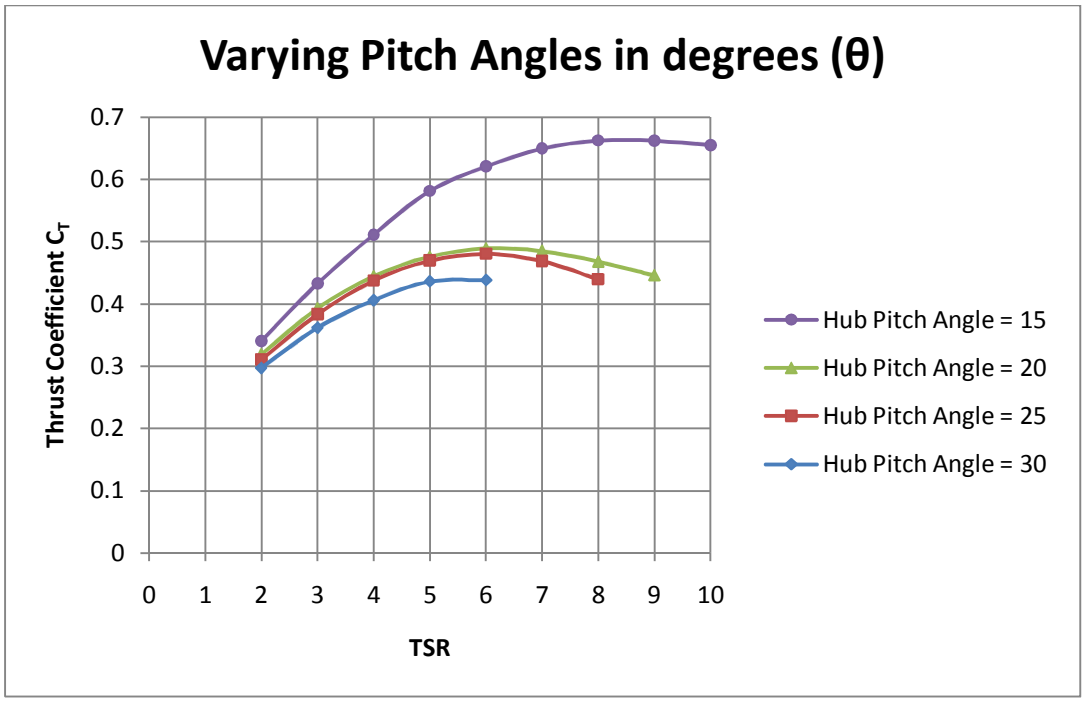

Figure 5.15 Thrust coefficients computed for a range of varying pitch angles and TSR for the COET ocean current turbine

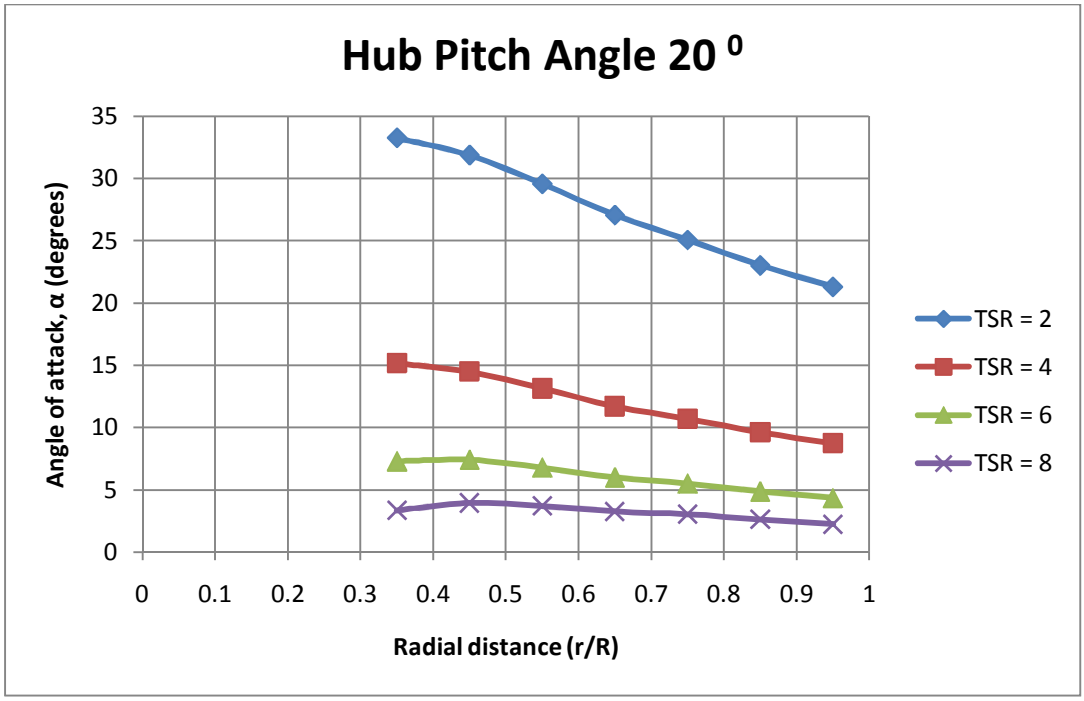

Figure 5.16 Radial variation of the angle of attack for a range of TSR for $\theta = 20^0$

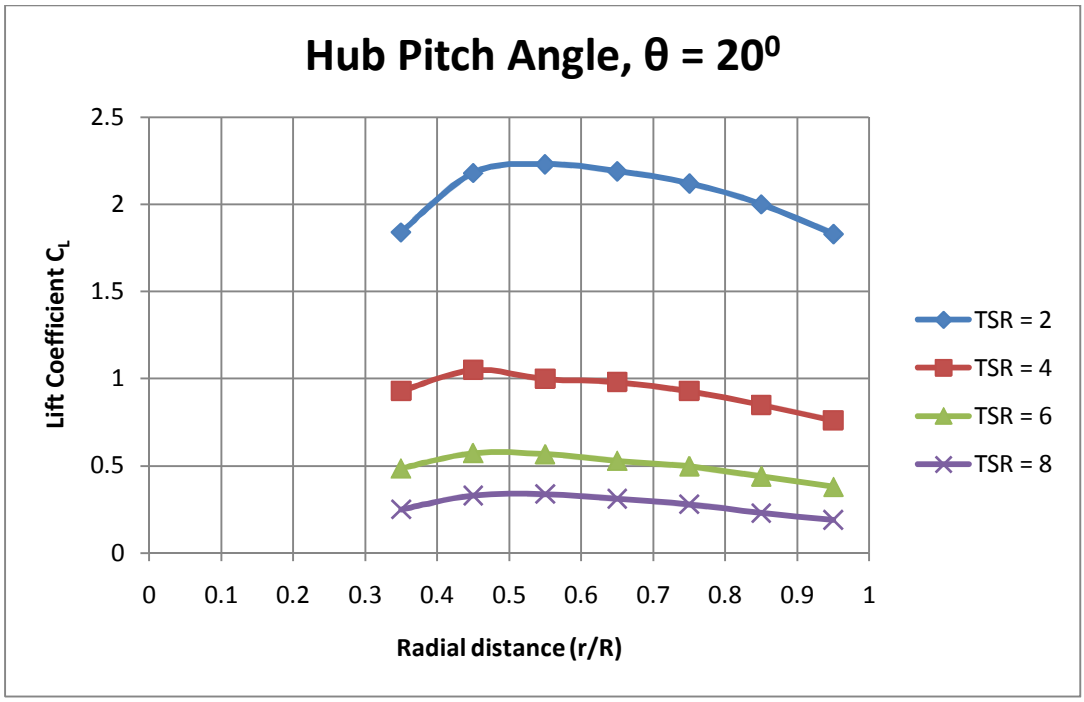

Figure 5.17 Radial variation of the lift coefficient for a range of TSR for $\theta = 20^0$

Pitch Angle\TSR	2	3	4	5	6	7	8
2^0	22.0	28.5	33.3	36.8	39.4	40.7	41.3
4^0	21.2	27.1	31.3	34.2	36.0	37.1	38.4
6^0	20.4	25.5	28.9	30.6	30.9	29.7	27.1
8^0	19.5	23.8	25.8	25.9	23.6	19.4	19.5

Table 5.1 Power computed in KW for a range of uniform pitch angles and TSR for the COET ocean current turbine

CHAPTER 6

CONCLUSION

In this research, we have developed a VLM algorithm to analyze flow about ocean current turbines. The validation study showed that the algorithm developed is quite accurate in that the results compared favorably with other published and experimental results. The VLM results compared satisfactorily with experimental results of Bahaj et al. [21] for a marine current turbine. VLM results obtained for the COET prototype current turbine show that

- A maximum power coefficient is achieved typically at tip speed ratio of 6
- The performance can be also significantly affected by radial variation of the pitch angle.

The VLM algorithm requires only a fraction of a minute on a typical laptop computer to execute one run. The algorithm is therefore particularly useful for design optimization in which one may have to consider many designs from different perspectives: structural, hydrodynamic, material, cost etc.

The present algorithm involves a few approximation and assumptions such as (i) requirement of the thin sections, (ii) small angle of attack, (iii) modeling of incident velocity on the turbine through induction factors determined from momentum and blade-

element theories etc. Future works may improve upon these assumptions and approximations. Also, in the present work the geometry of the trailing vortices is assumed. By carrying out unsteady simulation, in which the evolution of the trailing vortices is tracked, one can determine the exact steady state condition of trailing vortices and there by determine the performance of turbine more accurately. As future work, one could also extend the algorithm to include viscosity effects, in particular the viscous drag, in some empirical fashion so that the predicted results would be more realistic at large angle of attack. Using a vortex panel method (VPM) [14], in which both pressure and suction sides of a lifting surface are discretized and flow analyzed, flow about thick turbine blades can be modeled more accurately. By comparing the VLM and VPM results with that from CFD analysis of turbulent flow equations, one can assess the significance of viscosity and turbulence.

BIBLIOGRAPHY

[1] Stommel H.M., *The Gulf Stream: a physical and dynamical description*, Edition 2, University of California Press, 1976.

[2] NASA, "NASA SeaWiFS Project", NASA Sea-Viewing wide field-of –view sensor, http://oceancolor.gsfc.nasa.gov/SeaWiFS

[3] Philips, P, *The Gulf Stream*, USNA/Johns Hopkins, 2007. http://fermi.jhuapl.edu/student/phillips/

[4] Henry R.M., "On the Structure of deep Gulf Stream", *Journal of Marine Research*, pp.119-142, 1982.

[5] Johns W.E; Hogg N.G, "Western boundary Currents", *US National Report to International Union of Geodesy and Geophysics*, Pg 1311-1334, 1995.

[6] COET, "Centre for Ocean Energy Technology", Florida Atlantic University, http://www.coet.fau.edu

[7] Manwell J.F, McGowman J.G, Rogers L. A, *Wind Energy Explained: theory, design and application*, Wiley & Sons, 2002.

[8] Katz J., Plotkin A, *Low-Speed Aerodynamics*, Cambridge University Press, 2001.

[9] Bertin J. J, *Aerodynamics for Engineers*, Fourth Edition, Prentice Hall, 2002.

[10] Houghton E.L., Carpenter P.W., *Aerodynamics for Engineering Students*, Fifth Edition, Butterworth Heinemann, 2003.

[11] Anderson D. J, *Fundamentals of Aerodynamics*, McGraw-Hill, University of Michigan, Michigan, 1984.

[12] Reza A Z, Dissipation and Eddy mixing associated with flow past an Underwater Turbine, *Master's Thesis*, Department of Ocean and Mechanical Engineering, Florida Atlantic University, Proposed 2010.

[13] Newman J.N., *Marine Hydrodynamics*, MIT press, Cambridge, Massachusetts, 1977.

[14] Mason W.H., *Applied Computational Aerodynamics – Lecture Notes*, Department of Aerospace and Ocean Engineering, Virginia Polytechnic Institute and State University, Volume 1, Chapter 6, 1998.
http://www.aoe.vt.edu/~mason/Mason_f/CAtxtTop.html

[15] Weber J, Brebner G G, "Low-Speed Tests on 45-deg Swept-Back Wings," Part I, Her Majesty's Stationery Office (HMSO), Reports and Memoranda No. 2882, London, 1951.

[16] Melin T, A Vortex Lattice MATLAB Implementation for Linear Aerodynamic Wing Applications, *Master's Thesis*, Department of Aeronautics, Royal Institute of technology (KTH), 2000.

[17] Masquelier L. M, Application of the Vortex Lattice Method to Propeller Performance Analysis, *Master's Thesis*, Graduate Aeronautical Engineering, United States Air Force, Air Force Institute of Technology, 1982.

[18] Chung H-L, An Enhanced Propeller Design Program Based on Propeller vortex Lattice Lifting Line Theory, *Master's Thesis*, Department of Mechanical Engineering, Massachusetts Institute of Technology, 2007.

[19] Karamcheti K, *Principles of ideal-fluid aerodynamics*, Second Edition, R.E. Krieger Pub. Co., 1980.

[20] Clancy J. L, *Aerodynamics*, Wiley & Sons, University of Michigan, Michigan 1975.

[21] Bahaj A.S., Molland A.F., Chaplin J.R., Batten W.M.J., "Power and thrust measurements of marine current turbines under various hydrodynamic flow conditions in a cavitation tunnel and a towing tank", Science Direct, November 2005.

[22] Asseff N, Design and Finite Element Analysis of an Ocean Current Turbine, *Master's Thesis*, Department of Ocean and Mechanical Engineering, Florida Atlantic University, July 2009.

APPENDIX A
THE "1/4TH – 3/4TH" RULE FOR PLACING BOUND VORTEX AND CONTROL POINT IN A PANEL

This appendix gives the explanation of the ¼ - ¾ rule. Consider a flat plate as shown in Figure A.1. A single vortex is placed at point 'a' and the velocity is calculated at point 'b', called as control point. The spacing between the vortex and control point is determined by comparing the results with thin air foil theory (Mason [14]). The explanation of the ¼ - ¾ rule presented in [14] is reviewed in this appendix.

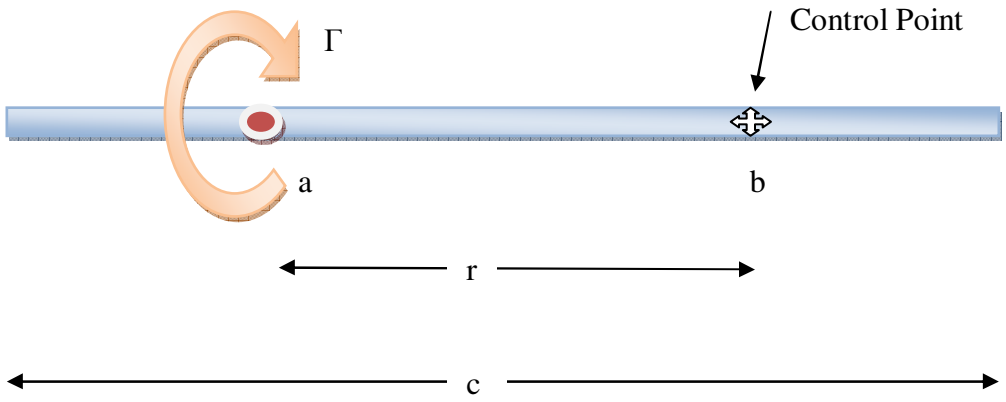

Figure A.1 Showing the position of vortex and control point for analysis

The velocity at the control point b, due to a vortex at a is:

$$v_b = -\frac{\Gamma}{2\pi r} \tag{A.1}$$

For small angles of attack and ignoring camber, the boundary condition as discussed earlier is:

$$v_b = V_\infty(-\alpha) \tag{A.2}$$

Now, Equating V_b in equations A.1 and A.2, we get

$$-\frac{\Gamma}{2\pi r} = -V_\infty \alpha \tag{A.3}$$

and therefore

$$\alpha = \frac{\Gamma}{2\pi r V_\infty} \tag{A.4}$$

Note that per Kutta-Joukowsky Theorem, lift force is given by

$$L = \rho V_\infty \Gamma \tag{A.5}$$

In terms of lift coefficient, lift force is given by

$$C_L = \frac{L}{\frac{1}{2}\rho {V_\infty}^2 c} \tag{A.6}$$

$$L = \frac{1}{2}\rho {V_\infty}^2 c.\, C_L \tag{A.7}$$

From the thin airfoil theory,

$$C_L = 2\pi\alpha \tag{A.8}$$

With above C_L in the equation A.7, we get for the lift force

$$L = \frac{1}{2}\rho {V_\infty}^2 c.\, 2\pi\alpha \tag{A.9}$$

With equation A.4 in A.9 and comparing with A.5, we get

$$\frac{1}{2}\rho {V_\infty}^2 c.2\pi.\frac{\Gamma}{2\pi r V_\infty} = \rho V_\infty \Gamma \tag{A.10}$$

$$\frac{1}{2}\frac{c}{r} = 1 \tag{A.11}$$

Thus,

$$r = \frac{c}{2} \tag{A.12}$$

Above provides the basis for placing the control point *b* at half-chord length from the vortex *a* in order to produce the theoretical lift of an airfoil predicted by thin airfoil theory. Next let us consider parabolic camber model to determine the placement of vortex.

Rewriting equation A.1 in terms of a and b, we get

$$v_b = -\frac{\Gamma}{2\pi(a-b)} \tag{A.13}$$

which with the kinematic boundary condition with camber becomes:

$$v_b = V_\infty\left(\frac{dz_c}{dx} - \alpha\right) \tag{A.14}$$

For a parabolic camber,

$$z_c(x) = 4\delta\left(\frac{x}{c}\right)(c-x) \tag{A.15}$$

and

$$\frac{z_c(x)}{dx} = 4\delta\left(1 - 2\left(\frac{x}{c}\right)\right) \tag{A.16}$$

Substituting the above equation in A.14 and equating it with the expressions A.13, we get

$$-\frac{\Gamma}{2\pi(a-b)} = V_\infty\left(4\delta\left(1 - 2\left(\frac{x}{c}\right)\right) - \alpha\right) \tag{A.17}$$

From the thin airfoil theory:

$$L = \frac{1}{2}\rho {V_\infty}^2 c.2\pi(\alpha + 2\delta) \tag{A.18}$$

Equating the above results for lift with Kutta-Joukowsky theorem (A.5), we obtain an expression for circulation strength of vortex as

$$\Gamma = \pi V_\infty c(\alpha + 2\delta) \tag{A.19}$$

With above in A.17, we obtain

$$\frac{-\pi V_\infty c(\alpha + 2\delta)}{2\pi(a-b)V_\infty} = 4\delta\left(1 - 2\left(\frac{x}{c}\right)\right) - \alpha \tag{A.20}$$

Upon satisfying the boundary condition at x = b, we get

$$-\frac{(\alpha + 2\delta)}{2}\left(\frac{c}{b-a}\right) = 4\delta\left(1 - 2\left(\frac{b}{c}\right)\right) - \alpha \tag{A.21}$$

For the above expression to be true for the arbitrary α, δ the coefficients must be equal; ie.,

$$-\left(\frac{c}{b-a}\right) = 4\left(1 - 2\left(\frac{b}{c}\right)\right) \tag{A.22}$$

$$-\frac{1}{2}\left(\frac{c}{b-a}\right) = -1 \tag{A.23}$$

Further simplifying the second equation we get:

$$(b-a) = \frac{c}{2} \tag{A.24}$$

which is the same as the result obtained earlier in A.12.

$$r = (b-a) = \frac{c}{2} \tag{A.25}$$

Now considering equation A.22 which is

$$-\left(\frac{c}{b-a}\right) = 4\left(1 - 2\left(\frac{b}{c}\right)\right) \tag{A.26}$$

And substituting equation A.25 in the above equation, we get

$$-\frac{1}{2} = 1 - 2\left(\frac{b}{c}\right)$$
$$\frac{b}{c} = \frac{3}{4} \tag{A.27}$$

With

$$(b - a) = \frac{c}{2}$$
$$\frac{b}{c} - \frac{a}{c} = \frac{1}{2} \tag{A.28}$$

we get

$$\frac{a}{c} = \frac{1}{4} \tag{A.29}$$

The above principle is called as the "¼ - ¾ rule", because the vortex is located at the ¼ chord point, and the control point is located at the ¾ chord point. It's not a theoretical law simply a basic for placing the bound vortex and the control point that works well and has become a rule of thumb. The ¼ - ¾ rule is widely used, and has proven to be sufficiently accurate in practice.

APPENDIX B
CALCULATION OF INDUCTION FACTORS a AND a'

The axial flow at the turbine is not exactly the far-field upstream current speed (as illustrated in Figure B.1). The axial and transverse components of the flow velocity specified on the vortice lattice panels can however be determined using the induction factors a and a' (Manwell [7]). The calculation of these factors, presented in [7], is reviewed in this appendix.

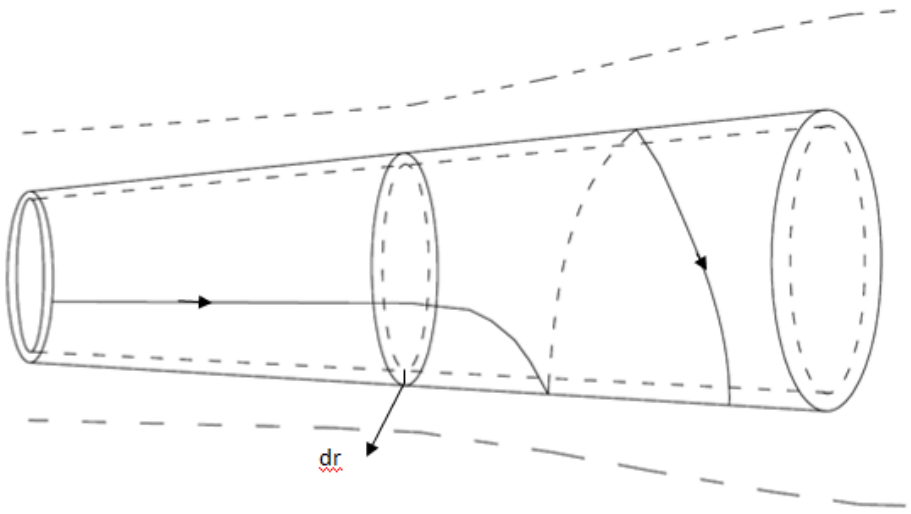

Figure B.1 Illustration of a flow line past a turbine

Figure B.2 describes about the axial stream tube around a turbine. Four stations are shown in the diagram, 1 some distance upstream of the turbine, 2 upstream face turbine blades, 3 downstream face of the turbine blades and 4 some distance downstream of the turbine.V_1, V_2, V_3, V_4 are the velocities at station 1, 2, 3 and 4. A_1, A_2, A_3, A_4 are the areas at the respective stations (sections). Because of the horizontal pressure variations, one observes a reduction in the velocity between free stream and rotor plane.

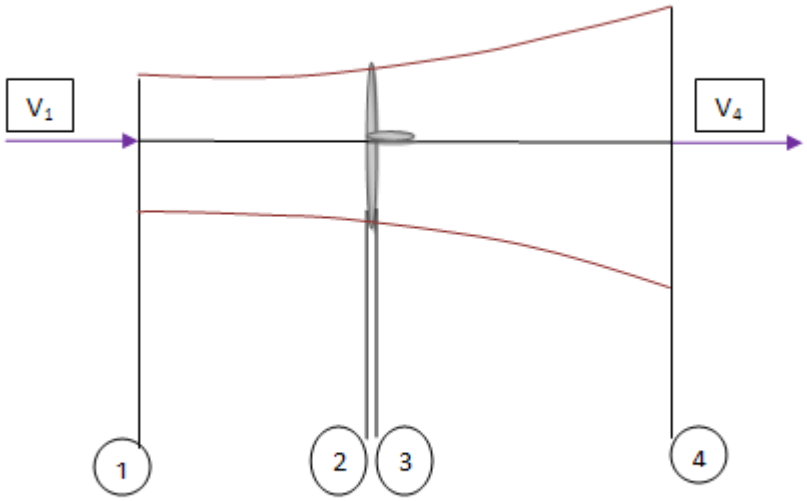

Figure B.2 Stream tube model of a turbine

The fractional decrease in velocity between the free stream and rotor plane is given by the axial induction factor (a):

$$V_2 = V_3 = V_1(1 - a) \qquad \text{(B.1)}$$

The method employed here for the determination of a uses blade element momentum (or BEM) theory. BEM theory is the combination of the momentum theory and blade element theory. The first method is to use a momentum balance on a rotating annular stream tube passing through a turbine. The second is to examine the forces generated by the aerofoil lift and drag coefficients at various sections along the blade. These two methods then give a series of equations that can be solved iteratively to get a and a'.

Momentum Theory:

Consider a turbine in the stream tube as shown earlier in Figure B.2 in this appendix. As there is jump in pressure across the turbine blade, the Bernoulli function is used in the two control volumes of the turbine blades.

In the stream tube upstream of the turbine blades:

$$P_{r1} + \frac{1}{2}\rho {V_1}^2 = Pr_2 + \frac{1}{2}\rho {V_2}^2 \tag{B.2}$$

In the stream tube downstream of the turbine blades:

$$Pr_3 + \frac{1}{2}\rho {V_3}^2 = Pr_4 + \frac{1}{2}\rho {V_4}^2 \tag{B.3}$$

Where Pr is the pressure and ρ is the density of the fluid.

Assuming $Pr_1 = Pr_4$ and $V_2=V_3$, From the above two equations we get

$$Pr_2 - Pr_3 = \frac{1}{2}\rho\left({V_1}^2 - {V_4}^2\right) \tag{B.4}$$

Thrust can also be expressed as pressure time's area:

$$dT = (Pr_2 - Pr_3)dA = \frac{1}{2}\rho\left({V_1}^2 - {V_4}^2\right)dA \tag{B.5}$$

Defining axial induction factor as

$$a = \frac{V_1 - V_2}{V_1} \tag{B.6}$$

we get,

$$V_2 = V_1(1 - a) \tag{B.7}$$

We also know that, $V_2 = \frac{V_1 + V_4}{2}$

Thus,

$$V_4 = 2.V_2 - V_1 = 2V_1(1 - a) - V_1$$
$$V_4 = V_1(1 - 2a) \tag{B.8}$$

Substituting the above two equations in equation B.5, yields

$$dT = \frac{1}{2}\rho {V_1}^2\{4a(1 - a)\}2\pi r dr \tag{B.9}$$

Next, consider the conservation of angular momentum in the annular stream tube. The blade wake rotates with an angular velocity ω and the blades rotate with an angular velocity of Ω as shown in Figure B.3. We know that:

Moment of inertia of an annulus, $I = mr^2$

Angular Moment, $L = I\omega$

Torque, $Q = \frac{dI\omega}{dt} = \frac{d(mr^2\omega)}{dt} = \frac{dm}{dt}r^2\omega$

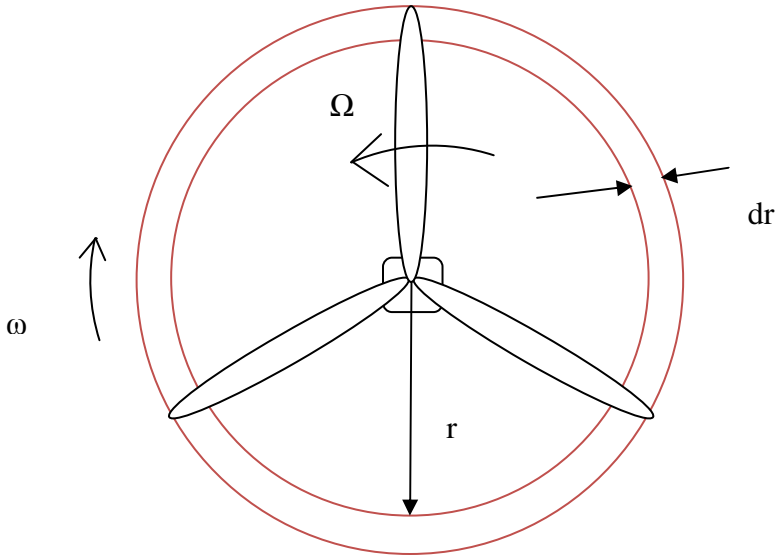

Figure B.3 Notation of an annular Stream tube

For a differential element corresponding torque is:

$$dQ = d\dot{m}\omega r^2 \tag{B.10}$$

For the rotating annular element

$$d\dot{m} = \rho A_2 V_2 \tag{B.11}$$

Thus,

$$dQ = \rho . 2\pi r dr . V_2 . \omega r^2 \tag{B.12}$$

The angular induction factor, a' is defined as:

$$a' = \frac{\omega}{2\Omega} \tag{B.13}$$

Substituting the equations B.7 and B.11 in the equation B.10 we get:

$$dQ = 4a'(1-a)\rho V_1 \pi r^3 \Omega dr \tag{B.14}$$

The above expressions, together with the Blade Element Theory which is discussed next, will be used in the VLM to find a and a' as explained in the later part of this appendix.

Blade Element Theory:

The forces on the blade of a turbine can also be expressed as a function of lift and drag coefficients and the angle of attack.

The two key assumptions in blade element theory are:

- The blade is composed of aerodynamically independent, narrow strips or elements.
- A differential blade element of chord C and width dr, located at a radius r form the rotor axis in considered as an airfoil section.

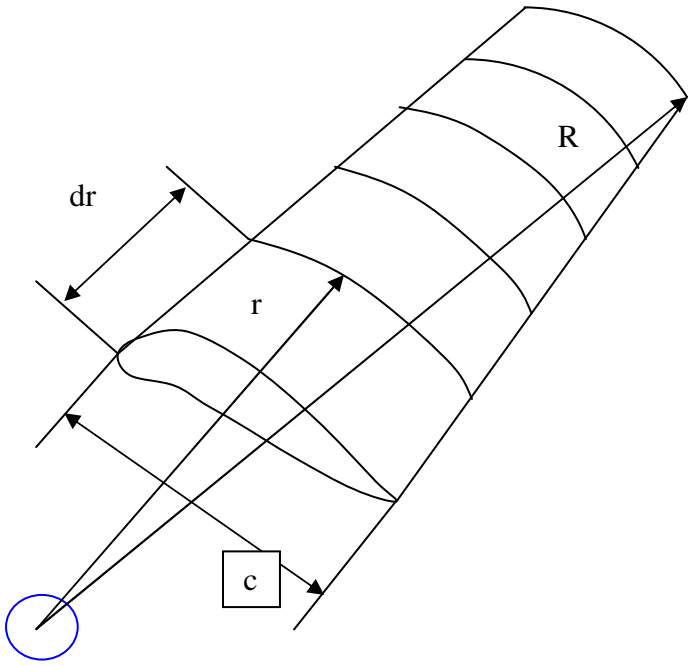

Figure B.4 Schematic of blade elements

Consider a blade divided up into 'n' elements as shown in Figure B.4. Each of the blade elements will experience a slightly different flow as they have a different twist angle (θ), a different chord length (c), a different rotational speed (Ωr) and different aerofoil characteristics. Numerical characteristics along the blade span yields the overall performance characteristics.

During the analysis of the forces on the blade section, it must be noted that the lift and drag forces are perpendicular and parallel, respectively to an effective, or relative velocity. The relative velocity is defined as the vector sum of the current velocity at the rotor, $V_1(1-a)$, and the velocity due to the rotation of the blade. This rotational velocity is the vector sum of the blade section velocity, Ωr, and the induced angular velocity at the blades from conservation of angular momentum, ωr/2, or

$$\Omega r + \frac{\omega r}{2} = \Omega r(1 + a') \tag{B.15}$$

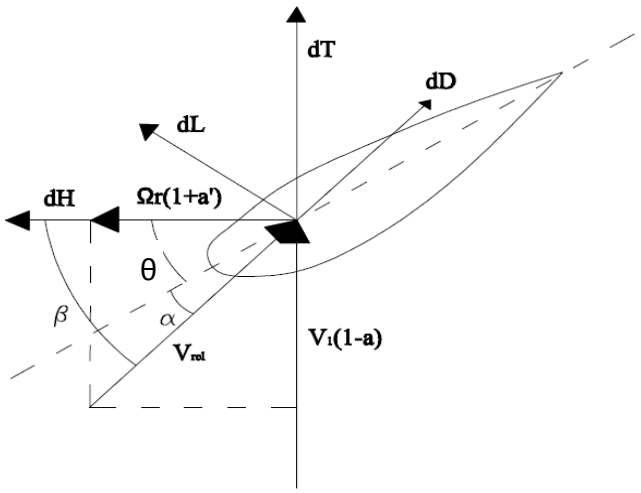

Figure B.5 Forces acting on turbine blade

Recalling from equation B.7, that $V_2=V_1$ (1-a) and from Figure B.5, we get

$$\tan\beta = \frac{V_1(1-a)}{\Omega r(1+a')} \tag{B.16}$$

The value of β varies from element to element in the blade. The local tip speed ratio λ_r is defined as:

$$\lambda_r = \frac{\Omega r}{V_1} \tag{B.17}$$

Thus the expression for β can also be written as:

$$\tan\beta = \frac{(1-a)}{\lambda_r(1+a')} \tag{B.18}$$

From Figure B.5, we note the following relations:

$$\alpha = \beta - \theta \tag{B.19}$$

$$V_{rel} = V_1(1-a)/\sin\beta \tag{B.20}$$

$$dL = C_L \frac{1}{2}\rho {V_{rel}}^2 c\, dr \tag{B.21}$$

$$dD = C_D \frac{1}{2}\rho {V_{rel}}^2 c\, dr \tag{B.22}$$

$$dT = dL\cos\beta + dD\sin\beta \tag{B.23}$$

$$dH = dL\sin\beta - dD\cos\beta \tag{B.24}$$

If the rotor has B blades, the total normal force on the blade section at a distance, r is:

$$dT = B\frac{1}{2}\rho {V_{rel}}^2 (C_L\cos\beta + C_D\sin\beta)cdr \tag{B.25}$$

The differential torque due to the tangential force operating at a distance, r is:

$$dQ = BrdH$$

$$dQ = B\frac{1}{2}\rho {V_{rel}}^2 (C_L \sin\beta - C_D \cos\beta) crdr \tag{B.26}$$

As an aside note, one can observe the effect of drag, from the above equations, which is to increase the thrust force and decrease the torque.

Expressing the above equations in terms of induction factors, β, etc, we get:

$$dT = \sigma' \pi \rho \frac{{V_1}^2 (1-a)^2}{sin^2\beta} (C_L \cos\beta + C_D \sin\beta) rdr \tag{B.27}$$

$$dQ = \sigma' \pi \rho \frac{{V_1}^2 (1-a)^2}{sin^2\beta} (C_L \sin\beta - C_D \cos\beta) r^2 dr \tag{B.28}$$

where σ' is called the local solidity and is defined by:

$$\sigma' = \frac{Bc}{2\pi r} \tag{B.29}$$

Blade Element Momentum Equations:

We now have four equations, two from momentum theory which expresses axial thrust and the torque.

$$dT = \frac{1}{2}\rho {V_1}^2 \{4a(1-a)\} 2\pi r dr \tag{B.30}$$

$$dQ = 4a'(1-a)\rho V_1 \pi r^3 \Omega dr \tag{B.31}$$

We also have two equations from the blade element theory from a consideration of blade forces which express the axial force and torque in terms of the aerodynamic coefficients.

$$dT = \sigma' \pi \rho \frac{{V_1}^2 (1-a)^2}{sin^2 \beta} (C_L \cos\beta + C_D \sin\beta) r dr \quad \text{(B.32)}$$

$$dQ = \sigma' \pi \rho \frac{{V_1}^2 (1-a)^2}{sin^2 \beta} (C_L \sin\beta - C_D \cos\beta) r^2 dr \quad \text{(B.33)}$$

Now let us equate equations B.30 and B.31 from momentum theory with equations B.32 and B.33 of blade element theory. Once this is done the following useful relation arise:

$$\frac{a}{1-a} = \frac{\sigma'(C_L \cos\beta + C_D \sin\beta)}{4sin^2\beta} \quad \text{(B.34)}$$

$$\frac{a'}{1-a} = \frac{\sigma'(C_L \sin\beta - C_D \cos\beta)}{4\lambda_r sin^2\beta} \quad \text{(B.35)}$$

The above two equations are used to find axial induction factor a and angular induction factor a'.

The procedure developed in the present thesis to determine a and a' is summarized below:

- Guess a and a'
- Determine Lambda and beta
- Find alpha, $\alpha = \beta - \theta$
- Find C_L and C_D from VLM code
- Again Calculate a and a' using equations B.34 and B.35
- Stop the iteration when Δa and Δa' are less than 0.001

Once a and a' values are obtained the current velocity at the blades and rotational velocity in the VLM code are replaced by V(1-a) and Ωr(1+a'). Thus, the quantities such as lift, induced drag, torque and power are computed from the VLM code.